

Rolling with Modular Symmetry: Quintessence and de Sitter in Heterotic Orbifolds

Hansel Gordillo–Ruiz¹, Miguel Hernández–Segura¹,
Ignacio Portillo–Castillo^{1,2}, Saúl Ramos–Sánchez¹ and Ivonne Zavala³*

¹*Instituto de Física, Universidad Nacional Autónoma de México, Cd. de México
C.P. 04510, México*

²*Facultad de Ingeniería, Universidad Autónoma de Chihuahua, Chihuahua
C.P. 31125, México.*

³*Centre for Quantum Fields and Gravity, Physics Department,
Swansea University SA2 8PP, UK*

Abstract

Modular invariance is a fundamental symmetry in string compactifications, constraining both the structure of the effective theory and the dynamics of moduli and matter fields. It has also gained renewed importance in the context of swampland conjectures and, independently, flavour physics. We investigate a modular-invariant scalar potential arising from heterotic orbifolds, where the flavour structure and moduli dynamics are jointly shaped by the underlying geometry. Focusing on a string-inspired, two-moduli truncation, we uncover a rich vacuum structure featuring anti-de Sitter minima and unstable de Sitter saddle points. We identify large regions in moduli space supporting multifield hilltop quintessence consistent with observations. All solutions satisfy refined swampland de Sitter bounds. Our results illustrate how modular symmetry can guide the construction of controlled, string-motivated quintessence scenarios within consistent effective theories.

*Electronic addresses

Contents

1	Introduction	2
2	Heterotic orbifold compactifications	4
2.1	Target space modular symmetry	5
2.1.1	The $\mathbb{T}^2/\mathbb{Z}_3$ orbifold	8
2.1.2	T' transformations of couplings and twisted matter	9
2.1.3	Modular T' from the $\mathbb{Z}_6 - \text{II}$ orbifold	10
2.1.4	Supersymmetric stabilisation of matter fields	11
2.2	Modular-Invariant Effective Action	12
2.2.1	The Kähler Potential	13
2.2.2	The Superpotential	13
2.2.3	The scalar potential	15
3	Mapping the modular de Sitter landscape	16
3.1	Properties of the critical points	21
3.1.1	Supersymmetry of adS minima	22
3.1.2	Unstable dS	22
3.1.3	Impact of modular invariance.	22
3.2	Tests on swampland conjectures	23
3.2.1	Refined dS conjecture	23
3.2.2	AdS scale separation	23
4	Multifield quintessence from modular dS saddles	24
4.1	Cosmological constraints on w_φ	29
4.2	The fate of dark energy: descent into adS	31
5	Discussion and Outlook	33
A	A concrete orbifold model	36
	References	39

1 Introduction

Heterotic orbifolds offer a remarkably fertile framework for deriving four-dimensional effective theories from string theory, combining realistic gauge structures with a deep intertwining of matter and moduli sectors [1–6]. In these models, compactifying the $E_8 \times E_8$ heterotic string on a toroidal orbifold T^6/P , where P is a discrete point group, yields chiral spectra, gauge symmetry breaking, and localized matter at orbifold fixed points. Crucially, such constructions inherit modular symmetries, remnants of target-space duality, which act non-trivially on both moduli and matter fields.

Far from being a residual geometric artifact, modular symmetry plays an active role in shaping effective theories from string compactifications. It constrains the structure of Yukawa couplings, governs the form of non-perturbative superpotentials, and serves as a guiding principle for constructing and validating complete low-energy effective field theories (LEEFTs).¹

More recently, modular symmetry has entered the stage of the swampland program (see [9, 10] for recent reviews). In [11], the unstable de Sitter (dS) vacua found in explicit heterotic orbifolds [7] were shown to satisfy the refined de Sitter swampland conjecture [12, 13], which imposes a universal bound on scalar potentials in consistent quantum gravities:

$$\frac{\sqrt{\nabla^i V \nabla_i V}}{V} \geq \frac{c}{M_{\text{Pl}}} \quad \text{or} \quad \frac{\min(\nabla^i \nabla_j V)}{V} \leq -\frac{c'}{M_{\text{Pl}}^2}, \quad (1)$$

where “min()” denotes the minimal eigenvalue and c and c' some $\mathcal{O}(1)$ positive constants. Subsequent work [14] further tested these constraints using modular-invariant potentials, again finding dS saddle points and maxima (but no dS minima) in line with [7, 11] and swampland expectations. Related developments have pointed to a modular-invariant formulation of the species scale [15–17] and its implications for entropy bounds and effective field theory cutoffs.

In parallel, modular symmetry has re-emerged in cosmology. In the early universe, modular-invariant inflation was proposed [18–24], and recently revived in the context of α -attractors and swampland constraints [25–28]. In the late universe, the latest results from the Dark Energy Spectroscopic Instrument (DESI) [29–33] and the Dark Energy Survey (DES) [34, 35] suggest that the current acceleration may be due to a *dynamical dark energy* (DDE). One popular possibility for such DDE is quintessence [36–38], described by a slowly rolling scalar.

¹Modular invariance was explicitly used to construct the full non-linear supergravity LEEFT in concrete heterotic orbifold models in [7]; a similar principle guided the derivation of anti-D3 uplifted flux compactifications in [8].

Despite its challenges, which include phantom crossings and the unresolved cosmological constant problem, DDE may offer a more natural string-theoretic origin than a positive cosmological constant. String-based models of exponential or hilltop quintessence have begun to emerge [39–41], and recent works [42–44] have pushed this dialogue between cosmology and the swampland further.

At the same time, a different motivation for modular symmetry has taken root: flavour. The proposal of [45] that finite modular groups might underlie lepton flavour structures has found a natural setting in heterotic orbifolds [46]. Recent studies have shown that modular transformations give rise to modular flavour symmetries [5, 47], which combine naturally with other moduli-independent symmetries of heterotic orbifolds, leading to the emergence of so-called eclectic flavour symmetries [46, 48, 49]. These symmetries place strong constraints on the LEEFT of the compactifications [50–52], enabling both the reproduction of experimental observations and the formulation of concrete predictions in flavour physics [53] via straightforward breaking patterns [54].

Flavour physics and moduli dynamics thus meet at a natural intersection in heterotic orbifolds. And yet, the interplay between these sectors, especially in the context of cosmological applications, remains largely unexplored. Our aim in this work is to take a step toward bridging this gap.

In this paper, we present a string-motivated model in which modular symmetry governs both the scalar potential for dynamical moduli and the flavour structure of matter fields. Our setup is based on the $\mathbb{T}^6/\mathbb{Z}_6 - \text{II}$ orbifold, whose geometry includes a $\mathbb{T}^2/\mathbb{Z}_3$ sector. This naturally gives rise to the finite modular group $\Gamma'_3 \cong T'$, which acts as a non-Abelian flavour symmetry on twisted-sector fields localised at fixed points.

Building on the explicit heterotic orbifold construction of [7], we construct a modular-invariant supergravity theory incorporating both double gaugino condensation and modular Yukawa couplings². We focus on scenarios with two dynamical moduli, the dilaton and a Kähler modulus; other moduli and matter fields are considered to develop vacuum expectation values (VEVs) while preserving supersymmetry at the compactification scale. This leads to a modular-invariant scalar potential suitable for studying both vacuum structure and cosmological dynamics.

Our results reveal a landscape populated by anti-de Sitter (adS) minima and dS saddle

²In the recent work [55], heterotic toroidal orbifold vacua for the overall Kähler modulus and the dilaton were investigated. That study incorporated non-perturbative corrections to both the superpotential and the Kähler potential, while preserving modular invariance. However, Yukawa couplings were not included, and only a single gaugino condensate was considered.

points³ consistent with swampland expectations as well as multifield rolling trajectories supporting hilltop quintessence⁴. In particular, we find large regions in moduli space where rolling trajectories along a single tachyonic direction cluster. While its full physical origin remains to be understood, its emergence may signal hidden modular patterns in the potential.

This work also realises the hilltop quintessence scenario of [11] in a fully modular setting, unifying string-derived flavour structure with rolling scalar dynamics. In doing so, it offers a new template for embedding late-time cosmology in UV-complete frameworks.

The paper is structured as follows. In Section 2, we review modular symmetries in heterotic orbifolds and their consequences for the effective theory. Section 3 presents the numerical landscape of vacua and dynamical solutions. Our analysis of multifield quintessence and cosmological trajectories appears in Section 4, followed by conclusions and future outlook in Section 5. In Section A we provide the details of a $\mathbb{T}^6/\mathbb{Z}_6 - \text{II}$ orbifold model used as a basis of our study. In the following, unless stated otherwise, we adopt the reduced Planck units with $M_{\text{Pl}} = 1$.

2 Heterotic orbifold compactifications

Toroidal heterotic orbifolds are a class of compactifications in which the extra six dimensions of a heterotic string are taken to be a quotient of a six-torus \mathbb{T}^6 by a discrete symmetry group. Explicitly, the compact space is defined as

$$\mathcal{O}_6 = \mathbb{T}^6/P, \tag{2}$$

where P is a finite group of discrete isometries of the torus, known as *point group*. To be compatible with the toroidal structure, P must act crystallographically on the underlying lattice Λ defining \mathbb{T}^6 , which we consider factorisable: $\mathbb{T}^6 = \mathbb{T}^2 \times \mathbb{T}^2 \times \mathbb{T}^2$. The point group acting on \mathbb{T}^6 is generated by $\text{SO}(6)$ rotations called twists, which in complex coordinates can be written as $\text{diag}(e^{2\pi i v_1}, e^{2\pi i v_2}, e^{2\pi i v_3})$, where $v = (v_1, v_2, v_3)^T$ is called twist vector.

It is often useful to instead define the orbifold in terms of its *space group* \mathcal{S} , which, in the absence of roto-translations, is given by the semidirect product

$$\mathcal{S} = P \ltimes \Lambda. \tag{3}$$

³Recent work on unstable dS solutions in string theory has appeared in [56–60].

⁴For recent work on multifield quintessence models see [61–67].

In this formulation, the orbifold is equivalently defined as a quotient of flat space by the space group,

$$\mathcal{O}_6 = \mathbb{R}^6/\mathcal{S}. \quad (4)$$

An important quality of an orbifold is that it is flat everywhere, but at a finite number of curvature singularities, which are those geometric points in \mathbb{R}^6 that are left fixed under the action of particular elements of \mathcal{S} .

The consistency of the heterotic strings demands the embedding of the orbifold \mathcal{O}_6 into the 16 gauge degrees of freedom. This can be done via a 16-dimensional shift vector V acting on the left-moving momenta. Focusing on the $E_8 \times E_8$ heterotic string, V shifts the momenta in the gauge lattice $\Lambda_{E_8 \times E_8}$ and thereby breaks down the gauge group $E_8 \times E_8$ to a 4-dimensional subgroup, which includes in many cases the gauge group of the Standard Model of particle physics (SM) [2, 4, 53, 68–70]. Twist and shift vectors must satisfy *modular invariance* constraints on the string worldsheet (see e.g. [1, 71–74] for more details).

The massless matter spectrum of a heterotic orbifold comprises two kinds of string states: *untwisted* and *twisted fields*. Untwisted matter fields are associated with those closed strings of the original string theory that are left invariant by the orbifold action. They are free to move in the bulk, the whole compact space. Twisted matter fields are related to strings that close only because of the (twist) action of the orbifold and are attached to the geometric fixed points of the orbifold. They all build various gauge representations, which, in realistic cases, include those of the SM quarks and leptons. Since the twisted states are linked to orbifold singularities, the replication of families may find an explanation in the number of fixed points of the orbifold.

2.1 Target space modular symmetry

The spectrum of states in an orbifold string compactification is invariant under target-space modular symmetry arising from T-duality [75–77], acting as discrete transformations on the moduli. Focusing on factorisable six-tori, each \mathbb{T}^2 includes two moduli: a complex structure U and a Kähler modulus τ . Under the orbifold action, the complex structure is geometrically fixed in all cases but $\mathbb{T}^2/\mathbb{Z}_2$ [49]. In contrast, the Kähler modulus τ is free and subject to a $SL(2, \mathbb{Z})$ target-space modular symmetry, which acts as⁵

$$\tau \xrightarrow{\gamma} \gamma\tau := \frac{a\tau + b}{c\tau + d}, \quad \gamma \in \Gamma, \quad (5)$$

⁵In the $\mathbb{T}^2/\mathbb{Z}_2$ case, the target-space duality group is $SL(2, \mathbb{Z})_\tau \times SL(2, \mathbb{Z})_U$ for null Wilson lines. In this work, we focus only on Kähler moduli as the complex structure is geometrically fixed in the case we shall consider (see [78] where the complex structure was also kept free).

where

$$\Gamma := \mathrm{SL}(2, \mathbb{Z}) = \left\{ \gamma := \begin{pmatrix} a & b \\ c & d \end{pmatrix} \mid a, b, c, d \in \mathbb{Z}, \quad ad - bc = 1 \right\}. \quad (6)$$

The generators of Γ can be chosen to satisfy the presentation

$$\langle S, T \mid (ST)^3 = S^4 = \mathbb{1}, TS^2 = S^2T \rangle \quad (7)$$

and are frequently represented by

$$S = \begin{pmatrix} 0 & 1 \\ -1 & 0 \end{pmatrix} \quad \text{and} \quad T = \begin{pmatrix} 1 & 1 \\ 0 & 1 \end{pmatrix}. \quad (8)$$

We see that τ transforms identically under both γ and $-\gamma$, which implies that τ only transforms non-trivially under $\mathrm{PSL}(2, \mathbb{Z}) = \Gamma/\mathbb{Z}_2$. Hence, the modulus τ takes values only in the upper half-plane

$$\mathcal{H} = \{ \tau \in \mathbb{C} \mid \mathrm{Im}(\tau) > 0 \}. \quad (9)$$

Further, the modular symmetry restricts the values of the modulus to the fundamental domain of Γ , which corresponds to the region illustrated in Figure 1. The modular transformations Γ leave three fixed points in the fundamental domain:

- $\tau = i$, fixed by S ;
- $\tau = \omega := e^{2\pi i/3}$, fixed by ST ; and
- $\tau = i\infty$, fixed by T .

There are interesting modular groups that can be obtained from the quotients of $\Gamma = \mathrm{SL}(2, \mathbb{Z})$ and its principal congruence subgroups $\Gamma(N)$, which are defined as

$$\Gamma(N) := \{ \gamma \in \Gamma \mid \gamma = \mathbb{1} \pmod{N} \}. \quad (10)$$

The quotient $\Gamma/\Gamma(N) =: \Gamma'_N$ is a so-called finite modular group of level N .

In general, associated with any congruence modular group, there are holomorphic functions of $\tau \in \mathcal{H}$ of level N , known as modular forms, which change under modular transformations according to

$$f_i(\tau) \xrightarrow{\gamma} f_i(\gamma\tau) = (c\tau + d)^{n_{f_i}} f_i(\tau), \quad \gamma = \begin{pmatrix} a & b \\ c & d \end{pmatrix} \in \Gamma(N), \quad (11)$$

where $n_{f_i} \in \mathbb{N}$ denotes the so-called modular weight of f_i and $(c\tau + d)^{n_{f_i}}$ is known as automorphy factor. Note that γ in Equation (11) is an element of $\Gamma(N)$ and not of Γ .

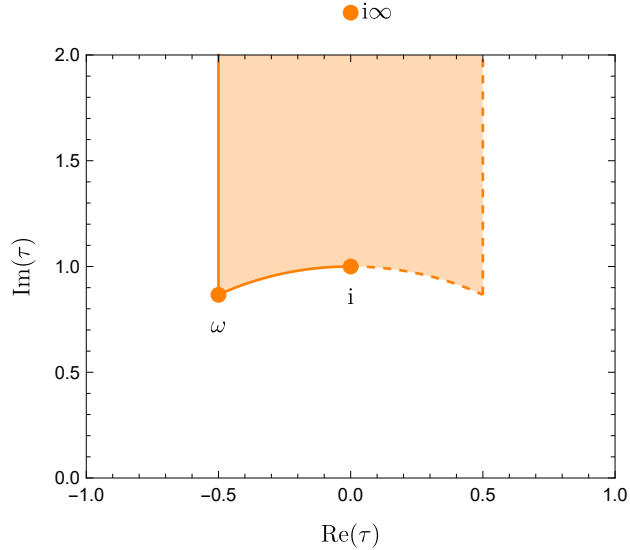


Figure 1: Fundamental domain of $SL(2, \mathbb{Z})$ for the modulus τ .

Indeed, under $\gamma \in \Gamma$ modular forms of level N and identical weight n_F transform non-trivially within finite-dimensional vector subspaces of modular forms. Considering one of these subspaces of dimension s , the vector $\hat{F}_{\mathbf{s}}^{(n_F)}(\tau) = (f_1(\tau), \dots, f_s(\tau))^T$ is a so-called vector-valued modular form (VVMF) [79] and transforms according to

$$\hat{F}_{\mathbf{s}}^{(n_F)}(\gamma\tau) \xrightarrow{\gamma} \hat{F}_{\mathbf{s}}^{(n_F)}(\gamma\tau) = (c\tau + d)^{n_F} \rho_{\mathbf{s}}(\gamma) \hat{F}_{\mathbf{s}}^{(n_F)}(\tau), \quad \gamma \in \Gamma, \quad (12)$$

with $\rho_{\mathbf{s}}(\gamma)$ a unitary irreducible s -dimensional representation of γ in the finite group Γ'_N . Similar properties hold for other finite modular groups resulting from the quotients of Γ and any of its normal subgroups (see e.g. [80–82] for examples).

On the other hand, since heterotic orbifolds are based on toroidal compactifications, it is natural to expect that some of these transformations arise naturally as target-space modular symmetries. In fact, it turns out that heterotic orbifolds exhibit finite modular groups as flavor symmetries of the LEEFT [46]. To uncover the modular symmetries that arise in heterotic orbifolds, it is useful to switch to the Narain description of the compactification of the heterotic string over an orbifold [83]. In this formalism, the outer automorphisms of the Narain space group⁶ encode the flavour symmetries of the LEEFT [5, 47, 49]. These automorphisms can be classified either as purely translational or rotational. The rotational outer automorphisms of the Narain space group precisely build the target-space modular symmetries of the theory. One can further show that these symmetries are

⁶Not to be confused with the space group \mathcal{S} in Equation (3). The Narain space group codifies both the geometric and the gauge degrees of freedom, providing a richer description of the compactification, see e.g. [84].

realised both by matter fields and their coupling strengths as finite modular groups. For instance, it is known that $\mathbb{T}^2/\mathbb{Z}_K$ orbifolds, $K = 2, 3, 4, 6$, lead respectively to the finite modular groups⁷ $(S_3 \times S_3) \rtimes \mathbb{Z}_4 \cong [144, 115]$, $\Gamma'_3 \cong T' \cong [24, 3]$, $2D_3 \cong S'_4/(\mathbb{Z}_2 \times \mathbb{Z}_2) \cong [12, 1]$, and $\Gamma'_6 \cong S_3 \times T' \cong [144, 128]$ [46, 52]. Invariance under these target-space modular symmetries imposes non-trivial constraints on the form of the allowed background fields, the symmetry properties of the matter fields, their couplings, and the consistency of the effective theory.

Under the action of the modular group, untwisted and twisted matter fields display similar transformations to those of VVMFs. Explicitly,

$$\Phi^{(n)} \xrightarrow{\gamma} \Phi^{(n)'} := (c\tau + d)^n \rho_r(\gamma) \Phi^{(n)}, \quad \gamma \in \Gamma, \quad (13)$$

where $(c\tau + d)^n$ is again an automorphy factor and $\rho_r(\gamma)$ is an r -dimensional matrix representation of γ in the finite modular group. Untwisted states transform as singlets of the finite modular group while twisted matter fields localised at the various orbifold singularities build r -dimensional field multiplets. Their modular weights n are determined by the geometric properties of the associated strings [86, 87]. While for untwisted fields they are either -1 or 0 , for twisted fields they possess various fractional values, which can be both positive and negative.

2.1.1 The $\mathbb{T}^2/\mathbb{Z}_3$ orbifold

In this work, we focus on the well-known example of the $\mathbb{T}^2/\mathbb{Z}_3$ orbifold, where the finite modular symmetry is $\Gamma'_3 \cong T'$, and modular properties of the LEEFT are well understood.

The $\mathbb{T}^2/\mathbb{Z}_3$ orbifold is produced by modding out a two-torus by a \mathbb{Z}_3 isometry generated by the twist $\theta = \exp(2\pi i/3)$. The resulting geometry is shown in Figure 2. Points that are inequivalent on the torus are identified under the action of θ , which leads to three orbifold fixed points. Further, the fundamental domain of the orbifold is only one third of the fundamental region of the torus.

Untwisted or bulk matter fields in four dimensions arise from the decomposition of the ten-dimensional gauge bosons A^M of $E_8 \times E_8$, with $M = 0, \dots, 9$. This decomposition depends on the directions wrapped by the orbifold:

- Considering that $M = 6, 7$ correspond to the $\mathbb{T}^2/\mathbb{Z}_3$ orbifold, the associated compact dimensions give rise to untwisted scalars with modular weight -1 , denoted by $\Phi^{(-1)}$.

⁷We provide in brackets the GAP Id, given by the program Groups, Algorithms, and Programming (GAP) [85]. The first number is the order of the finite group, the second is a counter.

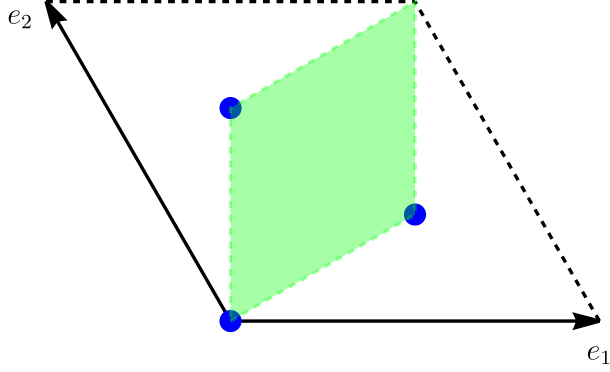


Figure 2: The $\mathbb{T}^2/\mathbb{Z}_3$ orbifold. The three inequivalent fixed points under the \mathbb{Z}_3 action are shown as blue dots. The green shaded region denotes the fundamental domain of the orbifold.

- The remaining compact directions $M = 4, 5, 8, 9$ yield the untwisted fields $\Phi^{(0)}$ with modular weight 0.

These untwisted matter fields are trivial singlets under the finite modular group T' .

The three fixed points of $\mathbb{T}^2/\mathbb{Z}_3$ host twisted strings, which are localised at those singularities. These states are associated with either the first or second twisted sectors, depending on whether the corresponding strings close under θ or θ^2 . Further, the states may include additional oscillator excitations, which modify their specific modular weights. Hence, the available twisted matter fields are

- $\Phi^{(-2/3)}$ and $\Phi^{(-5/3)}$ from the first twisted sector, and
- $\Phi^{(-1/3)}$, $\Phi^{(2/3)}$, $\Phi^{(-4/3)}$ and $\Phi^{(5/3)}$ from the second twisted sector.

The twisted matter states $\Phi^{(n)}$ include three massless fields each, which exhibit identical gauge quantum numbers.⁸ They can thus be considered flavour multiplets, with non-trivial transformations under the modular flavour symmetry T' . In the following, we discuss the details of these transformations and the properties of their couplings.

2.1.2 T' transformations of couplings and twisted matter

$\Gamma'_3 \cong T' \cong [24, 3]$ is generated by S and T, subject to the conditions

$$S^4 = \mathbb{1}, \quad (ST)^3 = \mathbb{1}, \quad S^2T = TS^2, \quad T^3 = \mathbb{1}, \quad (14)$$

⁸Note that this multiplicity offers an opportunity to explain the observed family repetition in the SM.

where the last relation renders the group finite. In this case, there are two modular forms, $\hat{Y}_1(\tau)$ and $\hat{Y}_2(\tau)$, with lowest modular weight $n_Y = 1$. They build a two-dimensional VVMF, transforming as a $\mathbf{2}''$ of T' [88], such that

$$\hat{Y}_{\mathbf{2}''}^{(1)}(\tau) = \begin{pmatrix} \hat{Y}_1(\tau) \\ \hat{Y}_2(\tau) \end{pmatrix} := \begin{pmatrix} -3\sqrt{2}\frac{\eta^3(3\tau)}{\eta(\tau)} \\ 3\frac{\eta^3(3\tau)}{\eta(\tau)} + \frac{\eta^3(\tau/3)}{\eta(\tau)} \end{pmatrix}, \quad (15)$$

with $\eta(\tau)$ the well-known Dedekind η function, defined as

$$\eta(\tau) = q^{\frac{1}{24}} \prod_{n=1}^{\infty} (1 - q^n) = q^{\frac{1}{24}} \sum_{n=-\infty}^{\infty} (-1)^n q^{\frac{1}{2}n(3n-1)}, \quad (16)$$

where $q := \exp(2\pi i\tau)$. From Equation (12) we observe that $\hat{Y}_{\mathbf{2}''}^{(1)}$ transforms under $\gamma \in \text{SL}(2, \mathbb{Z})$ as

$$\hat{Y}_{\mathbf{2}''}^{(1)}(\tau) \xrightarrow{\gamma} \hat{Y}_{\mathbf{2}''}^{(1)}(\gamma\tau) = (c\tau + d)^1 \rho_{\mathbf{2}''}(\gamma) \hat{Y}_{\mathbf{2}''}^{(1)}(\tau) \quad (17)$$

with $\rho_{\mathbf{2}''}(\text{S})$ and $\rho_{\mathbf{2}''}(\text{T})$ given by [52]

$$\rho_{\mathbf{2}''}(\text{S}) := -\frac{i}{\sqrt{3}} \begin{pmatrix} 1 & \sqrt{2} \\ \sqrt{2} & -1 \end{pmatrix} \quad \text{and} \quad \rho_{\mathbf{2}''}(\text{T}) := \begin{pmatrix} \omega & 0 \\ 0 & 1 \end{pmatrix}. \quad (18)$$

VVMFs $\hat{Y}_s^{(n_Y)}(\tau)$ with higher weights, $n_Y > 1$, can be straightforwardly constructed from tensor products of $\hat{Y}_{\mathbf{2}''}^{(1)}$; e.g. $\hat{Y}_{\mathbf{3}}^{(2)} = \hat{Y}_{\mathbf{2}''}^{(1)} \otimes \hat{Y}_{\mathbf{2}''}^{(1)}$, where the singlet disappears because it is antisymmetric. A crucial observation in heterotic orbifolds (and other string constructions) is that the couplings among string fields are, in fact, modular forms [89, 90]. Hence, since string couplings build non-trivial T' representations, so should string matter multiplets $\Phi^{(n)}$ in order to arrive at a modular-invariant LEEFT.

By using conformal field theory (CFT) techniques, it is possible to uniquely determine the representations of twisted matter fields [5, 47]. In particular, as summarised in Table 1, one finds that each multiplet of matter fields from the first twisted sector transforms as a $\mathbf{2}' \oplus \mathbf{1}$ of T' , while field multiplets from the second twisted sector transform as $\mathbf{2}'' \oplus \mathbf{1}$ [46]. The doublet representations of the T' generators acting on these fields are given by Equation (18) and

$$\rho_{\mathbf{2}''}(\text{S}) := -\frac{i}{\sqrt{3}} \begin{pmatrix} 1 & \sqrt{2} \\ \sqrt{2} & -1 \end{pmatrix} \quad \text{and} \quad \rho_{\mathbf{2}''}(\text{T}) := \begin{pmatrix} 1 & 0 \\ 0 & \omega^2 \end{pmatrix}. \quad (19)$$

2.1.3 Modular T' from the $\mathbb{Z}_6 - \text{II}$ orbifold

There are six different \mathbb{Z}_6 supersymmetric orbifolds in six dimensions [91]. Among them, the so-called $\mathbb{Z}_6 - \text{II}$ (1, 1) orbifold features a factorised structure as $\mathbb{T}^2/\mathbb{Z}_6 \otimes \mathbb{T}^2/\mathbb{Z}_3 \otimes \mathbb{T}^2/\mathbb{Z}_2$,

sector:	untwisted		first twisted		second twisted			
string state	$\Phi^{(0)}$	$\Phi^{(-1)}$	$\Phi^{(-2/3)}$	$\Phi^{(-5/3)}$	$\Phi^{(-1/3)}$	$\Phi^{(2/3)}$	$\Phi^{(-4/3)}$	$\Phi^{(5/3)}$
T' irrep	1		$2' \oplus 1$		$2'' \oplus 1$			

Table 1: Modular properties of matter multiplets of the $\mathbb{T}^2/\mathbb{Z}_3$ orbifold by sector [46].

which has been shown to be phenomenologically fruitful (see e.g. [7, 68, 92, 93]). This structure is particularly relevant for models of physics based on modular symmetries as the second torus offers a finite modular symmetry $\Gamma'_3 \cong T'$, which together with a traditional flavour symmetry renders promising predictions for quarks and leptons [53].

By e.g. using the `orbifolder` [3], one can show that the matter spectrum of $\mathbb{Z}_6 - \text{II}(1, 1)$ orbifolds offers both SM matter and gauge singlets transforming as described in Table 1. Most of these states are $\Phi^{(-2/3)}$ fields, whose couplings have been explicitly studied before [52]. In particular, as we shall describe shortly, it is known that the modular forms $\hat{Y}_i(\tau)$ given in Equation (15) appear in the trilinear couplings $\Phi_\alpha^{(-2/3)} \otimes \Phi_\beta^{(-2/3)} \otimes \Phi_\gamma^{(-2/3)}$ in the LEEFT of these orbifolds, rendering the action modular invariant and thus providing a source for the (stabilising) potential of the modulus τ . We shall base our study on these properties.

In accordance with the general framework of $\mathbb{T}^2/\mathbb{Z}_K$ orbifolds [46], one might expect the associated LEEFT of $\mathbb{Z}_6 - \text{II}(1, 1)$ orbifolds to exhibit additional non-Abelian modular symmetries beyond T' . Interestingly, all semi-realistic models based on the $\mathbb{Z}_6 - \text{II}(1, 1)$ orbifold incorporate Wilson lines [4, 94], which in many cases are associated with the $\mathbb{T}^2/\mathbb{Z}_2$ orbifold sector. Since these background fields explicitly break the modular symmetries of the orbifold sectors to which they are coupled [95, 96], no non-Abelian modular symmetry can arise from the third torus. However, the $\mathbb{T}^2/\mathbb{Z}_6$ orbifold sector yields a $\Gamma'_6 \cong S_3 \times T'$ finite modular symmetry, under which (only) a few matter fields transform as doublets. For simplicity, since T' appears as part of the modular symmetry of the Kähler modulus τ_1 of $\mathbb{T}^2/\mathbb{Z}_6$ too, we shall assume that it can be stabilised by using the same mechanism we describe here; hence, we shall not discuss it explicitly in the following.

2.1.4 Supersymmetric stabilisation of matter fields

Prior to describing the specifics of the LEEFT that characterises our model, let us explain how matter fields $\Phi_\alpha^{(n_\alpha)}$ can be supersymmetrically stabilised. This is possible because scalar fields can naturally acquire VEVs when demanding supersymmetry at very large energies. To see this, we must recall that heterotic orbifolds exhibit a $U(1)_{\text{anom}}$, which induces a Fayet–Iliopoulos (FI) D -term [97] $\xi_{\text{FI}} \propto \sum_\alpha q_\alpha^{\text{anom}} > 0$ (the sign can always be

chosen this way). Hence, the complete D_{anom} term is

$$D_{\text{anom}} = \xi_{\text{FI}} + \sum_{\alpha} g_{\alpha}^{\text{anom}} |\Phi_{\alpha}^{(n_{\alpha})}|^2. \quad (20)$$

To retain supersymmetry at or close to the compactification scale, one must demand $\langle D_{\text{anom}} \rangle = 0$, which leads to non-vanishing VEVs, $\langle \Phi_{\alpha}^{(n_{\alpha})} \rangle$. Furthermore, it is known that also the F -terms can be simultaneously cancelled with D -flat VEV configurations (while also $\langle W \rangle \sim 0$) [98–100]. Due to the large amount of fields solving these equations, there is enough freedom to fix by hand some of the VEVs without significantly affecting the results. However, it could be interesting to study this in detail, which will be done in an extension of this work.

This assumption has various consequences. As mentioned before, exotic matter decouples at the scale of the VEVs and some extra (gauge and flavour) symmetries are spontaneously broken. In addition, as we shall shortly see, the effective action can be simplified. Further, in certain scenarios based on modular flavour symmetries, matter VEVs can even be instrumental to achieve realistic configurations allowing for dS vacua [101].

2.2 Modular-Invariant Effective Action

At energies well below the compactification scale, the LEEFT describing the dynamics of moduli and matter fields in heterotic orbifold compactifications is captured by a four-dimensional $\mathcal{N} = 1$ supergravity theory. The effective action is fully specified by the Kähler potential K , superpotential W , and gauge kinetic functions f_a , all of which are subject to stringent constraints from target-space modular invariance. This discrete symmetry, inherited from the underlying two-dimensional conformal field theory, governs the transformation properties of the moduli and the matter fields, ensuring consistency of the full quantum theory.

To preserve modular invariance, the functions K , W , and f_a must transform covariantly under modular transformations. In particular, the scalar potential derived from these quantities must remain invariant under the full modular group or its congruence subgroups, depending on the compactification geometry.

In addition, the modular symmetry may be anomalous at the quantum level. The mixed modular-gauge anomalies are cancelled via a Green–Schwarz (GS) mechanism [86, 102], which induces a non-trivial modular transformation for the dilaton:

$$S \mapsto S - \frac{\delta_{\text{GS}}}{8\pi^2} \log(c\tau + d), \quad (21)$$

where δ_{GS} is the universal GS coefficient and τ is the relevant Kähler modulus transforming under the modular group $\text{SL}(2, \mathbb{Z})$. The remaining anomaly is cancelled by threshold corrections from massive string states.

Under $\gamma \in \text{SL}(2, \mathbb{Z})$, the Kähler potential and the superpotential transform as

$$K \xrightarrow{\gamma} K + \log |c\tau + d|^2, \quad W \xrightarrow{\gamma} \frac{W}{(c\tau + d)}, \quad (22)$$

so that the Kähler-invariant function $G = K + \ln |W|^2$ and the scalar potential remain invariant. Modular forms with definite weights (n) are instrumental to construct modular-invariant quantities in the effective theory.

2.2.1 The Kähler Potential

The Kähler potential encodes the kinetic terms for both moduli and matter fields. For the untwisted Kähler modulus τ and the dilaton S , the Kähler potential including one-loop effects, takes the form [7]

$$K = -\log \left[S + \bar{S} - \frac{1}{8\pi^2} \delta_{\text{GS}} \log (i\bar{\tau} - i\tau) \right] - \log (i\bar{\tau} - i\tau). \quad (23)$$

Here, we do not display the matter contributions, as they may be considered negligible in the large-volume and small matter-field VEV limit, which we adopt here (see Section A for the complete expression). Twisted matter fields $\Phi_\alpha^{(n_\alpha)}$ localised at orbifold fixed points transform under the modular symmetry with definite modular weights n_α as specified in Equation (13).

2.2.2 The Superpotential

The superpotential receives two key contributions: Yukawa couplings from matter-field interactions and non-perturbative terms from gaugino condensates. Both ingredients are tightly constrained by modular symmetry.

Yukawa interactions. In heterotic orbifolds, Yukawa couplings are constrained by string selection rules [103–105] (see also [106] for non-Abelian orbifolds) and modular (flavour) symmetries [46, 50–52, 107]. These couplings can be computed explicitly from worldsheet CFT correlators and typically exhibit modular weight dependence. In particular, considering twisted matter fields of the type $\Phi_\alpha^{(-2/3)}$, the leading T' -invariant trilinear couplings arise from

$$W \supset \left(\hat{Y}_{\mathbf{2}''}^{(1)}(\tau) \otimes \Phi_\alpha^{(-2/3)} \otimes \Phi_\beta^{(-2/3)} \otimes \Phi_\gamma^{(-2/3)} \right)_1, \quad (24)$$

whose explicit expression is given in Section A, see Equation (63). Once the matter fields acquire VEVs, the effective Yukawa superpotential is given by

$$W_{\text{Yuk}} = -\frac{1}{\sqrt{2}}\tilde{\lambda}_1\hat{Y}_1(\tau) + \tilde{\lambda}_2\hat{Y}_2(\tau) + \dots, \quad (25)$$

where $\hat{Y}_i(\tau)$ are modular forms defined in Equation (15), and the coefficients $\tilde{\lambda}_i$ parameterise the matter VEVs. These coefficients take the general form $\tilde{\lambda}_i \propto \langle\Phi_{\alpha,p}\rangle\langle\Phi_{\beta,q}\rangle\langle\Phi_{\gamma,r}\rangle$ up to some known coefficients and (gauge and flavour) singlet VEVs, with $\Phi_{\alpha,p}$, $p = 1, 2, 3$, the components of $\Phi_\alpha^{(-2/3)}$. The factor $-1/\sqrt{2}$ in the first term shows the relative coupling strength between matter fields localised at the same fixed point and those localised at three different fixed points. This ratio is fixed by demanding invariance under the additional $\Delta(54)$ symmetry, which is present in these constructions [52].

Non-perturbative contributions. Gaugino condensation in hidden sector gauge groups $G_a \subset E_8 \times E_8$ generates non-perturbative superpotential terms of the form [77]

$$W_{\text{gc}}^{(a)} \sim e^{-\frac{8\pi^2}{b_a}f_a(S,\tau)}, \quad (26)$$

where b_a is the one-loop beta function coefficient of G_a , and f_a is the gauge kinetic function. At tree-level, $f_a = k_a S$, but one-loop threshold corrections introduce moduli dependence:

$$f_a = k_a S + \frac{1}{4\pi^2}\Delta_a(\tau), \quad (27)$$

with $\Delta_a(\tau)$ containing modular functions that transform appropriately to cancel anomalies and ensure covariance of the full non-perturbative term.

Phenomenologically viable models are known to frequently display multiple gaugino condensates, as shown in explicit heterotic orbifold constructions [7]. Hence, we consider a model with two gauge sectors condensing independently. We parameterise these non-perturbative effects from double gaugino condensation following [77] as

$$W_{\text{gc}} = \frac{\Omega_1(S)H_1(\tau)}{\eta^2(\tau)} + \frac{\Omega_2(S)H_2(\tau)}{\eta^2(\tau)}, \quad (28)$$

with $\eta(\tau)$ the Dedekind eta function defined in Equation (16) and $H_a(\tau)$ are the most general modular invariant functions without singularities in the fundamental domain, parameterised by [108, 109]

$$H_a(\tau) = \left(\frac{E_4(\tau)}{\eta^8(\tau)}\right)^{n_a} \left(\frac{E_6(\tau)}{\eta^{12}(\tau)}\right)^{m_a} P(j(\tau)) = (j(\tau) - 1728)^{m_a/2} j(\tau)^{n_a/3} P(j(\tau)), \quad (29)$$

where n_a, m_a are some non-negative integers, P is a polynomial function of the Klein invariant function $j(\tau)$ given by

$$j(\tau) = 1728 \frac{E_4(\tau)^3}{E_4(\tau)^3 - E_6(\tau)^2}. \quad (30)$$

Here, $E_4(\tau)$ and $E_6(\tau)$ are the Eisenstein series of weight 4 and 6, respectively, defined as

$$E_4(\tau) := 1 + 240 \sum_{n=1}^{\infty} \frac{n^3 q^n}{1 - q^n} \quad \text{and} \quad E_6(\tau) := 1 - 504 \sum_{n=1}^{\infty} \frac{n^5 q^n}{1 - q^n}. \quad (31)$$

Finally, $\Omega_a(S)$ are functions of the dilaton given by [7]

$$\Omega_a(S) := \frac{c_a}{e} \frac{b_a^0}{96\pi^2} \exp \left[\frac{24\pi^2}{b_a^0} f_a \right], \quad (32)$$

where e is the Euler number, c_a are unknown constants taken for convenience here as $c_1 = 1$, $c_2 = 8\pi^2 e$. Further, f_a are the 1-loop gauge kinetic functions

$$f_a = k_a S - \frac{b_a - b_a^0}{8\pi^2} \log M_d \quad (33)$$

in terms of the level k_a of the Kač-Moody algebra, the scale M_d at which all extra (exotic) matter fields are decoupled, the beta-function coefficient b_a that includes charged matter, and the beta-function coefficient of the pure Yang-Mills theory.

2.2.3 The scalar potential

We now have all the ingredients to write down the F-term of the potential for the moduli we consider. This is given by

$$V = e^K \left[K^{A\bar{B}} D_A W D_{\bar{B}} \bar{W} - 3|W|^2 \right], \quad (34)$$

where A, B denote all fields present and $D_A W = \partial_A W + \partial_A K W$, with

$$W = W_{\text{Yuk}} + W_{\text{gc}}. \quad (35)$$

Using the Kähler potential in Equation (23) and defining the auxiliary function $Y := S + \bar{S} - \frac{1}{8\pi^2} \delta_{\text{GS}} \log(i\bar{\tau} - i\tau)$, the moduli scalar potential can be written as

$$V = e^K \left[|Y W_S - W|^2 + \frac{Y}{Y - \frac{\delta_{\text{GS}}}{8\pi^2}} \left| \frac{\delta_{\text{GS}}}{8\pi^2} \left(\frac{2W}{Y} - W_S \right) + i(i\bar{\tau} - i\tau) W_{\tau} - W \right|^2 - 3|W|^2 \right]. \quad (36)$$

With the effective $\mathcal{N} = 1$ supergravity theory fully specified and the F-term scalar potential explicitly constructed, we are now in a position to investigate the vacuum structure of the model. Given the complexity of the scalar potential and the presence of multiple moduli with nontrivial couplings, we employ numerical techniques in order to explore the landscape of solutions and identify stable vacua and other physically interesting critical points consistent with the symmetries and constraints of the compactification.

3 Mapping the modular de Sitter landscape

We now proceed to chart the modular-invariant heterotic orbifold landscape, drawing on the scalar potential defined in Section 2.2, Equation (36), and examine the distribution of unstable de Sitter saddles, stable adS vacua, and other critical points throughout moduli space.

We assume that the matter fields acquire VEVs of the same order, taken to be $\mathcal{O}(10^{-1})$ so as to remain within the regime of validity of the Kähler potential calculation. Such VEVs can lead to the parameter values $\tilde{\lambda}_1 = 3/25000$ and $\tilde{\lambda}_2 = 3/5000000$ in Equation (25). We also set $c_1 = 1$ and $c_2 = 8\pi^2 e$, so that the coefficients in Equation (32) differ in magnitude.⁹

The parameters b_1 , b_1^0 , and δ_{GS} are computed from the explicit orbifold model described in Section A for one $SU(3)$ factor, while b_2 and b_2^0 are chosen to ensure that the second condensate becomes dominant at a different order in moduli expansion. Since the Kač-Moody level is $k = 1$ for standard heterotic orbifold models, we take $k_1 = k_2 = 1$. The decoupling scale M_d must lie not far below the Planck scale;¹⁰ here we fix it to be $M_d = 1/65$. Given these choices, the detailed structure of the critical points is controlled by the integers m_a , n_a and by the polynomial $P(j(\tau))$ in the modular invariant functions (29), for computational simplicity, the polynomial was fixed¹¹ as $P(j(\tau)) = 1$ and m_a , n_a were taken¹² within $[0, 12]$. All parameter values used in our analysis are summarised in Table 2.

$\tilde{\lambda}_1$	$\tilde{\lambda}_2$	c_1	c_2	b_1	b_2	b_1^0	b_2^0	M_d	k_1	k_2	δ_{GS}
3/25000	3/5000000	1	$8\pi^2 e$	5	-26	-9	-12	1/65	1	1	-1

Table 2: Parameter values for the numerical search.

Let us first provide an overview of our procedure to classify the physics of our model. We explore various criteria to identify phenomenologically relevant critical points of the scalar potential of Equation (36). To analyse them, we implement a hierarchical classification scheme that helps better understand their properties. The procedure, summarised in Figure 3, begins by locating critical points, where the gradient ∇V approximately vanishes.

In detail, our search for critical points employs both `Mathematica` and `Python` im-

⁹These values represent a convenient choice and are not unique; however, we have explicitly verified that reasonable variations of c_1 and c_2 do not modify the qualitative features of our results.

¹⁰As shown in [98], exotic matter can decouple a few orders of magnitude below the Planck scale.

¹¹Other choices may modify the shape of the potential, leading to other results. However, studying all the possible choices for $P(j(\tau))$ is beyond the scope of this work.

¹²Since $H(\tau)$ is a holomorphic singularity-free function in the fundamental domain, it admits a locally convergent series expansion. Hence, taking higher values for n_a and m_a yields contributions that are negligible compared to those from smaller values.

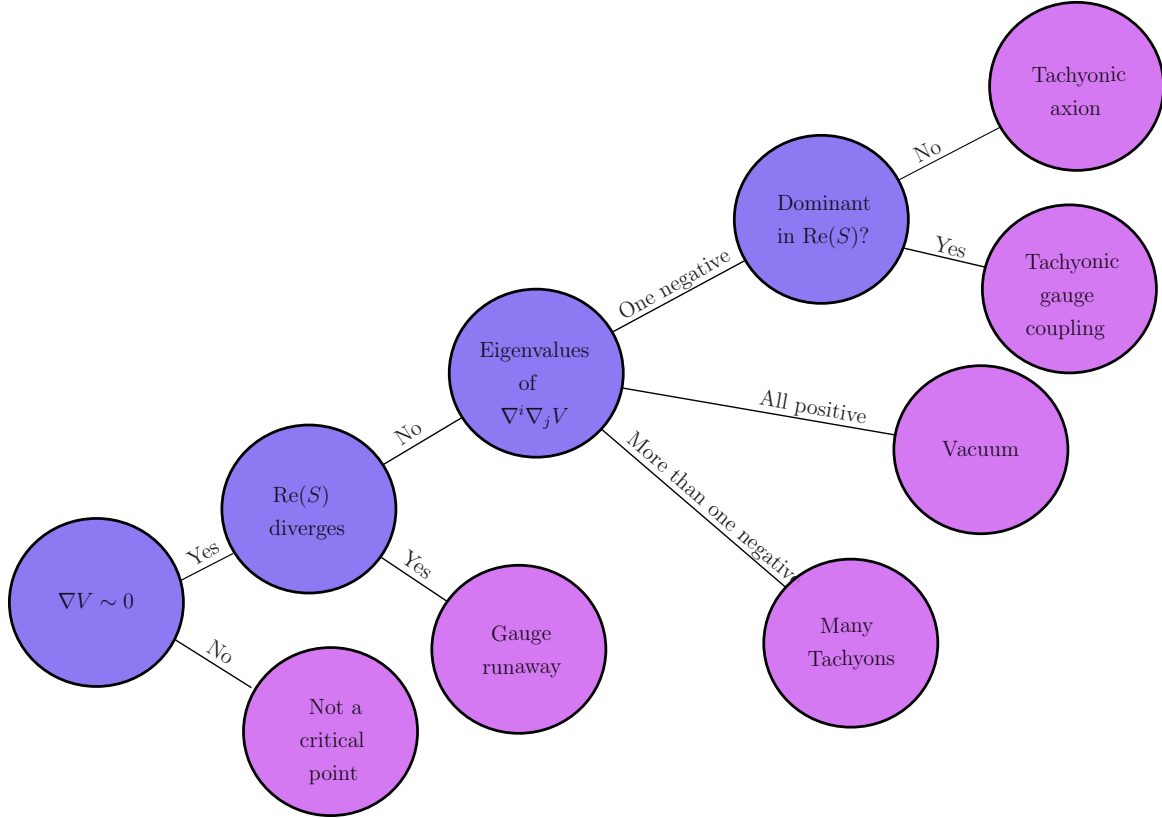


Figure 3: Hierarchical classification scheme applied to critical points of the scalar potential V , based on their properties. Initial filtering identifies candidate critical points where $\nabla V \sim 0$. Then, we discriminate the cases where $\text{Re}(S)$ diverges. The eigenvalues of the Hessian $\nabla^i \nabla_j V$ are then evaluated to assess the stability of each solution: cases with all positive eigenvalues, one negative eigenvalue, or multiple negative eigenvalues are distinguished. We then evaluate whether the dominant contribution arises from $\text{Re}(S)$. Based on the outcomes of these filters, each point is assigned to a physical class: *Vacuum*, *Gauge runaway*, *Many tachyons*, *Tachyonic axion*, *Tachyonic gauge coupling*, or *Not a critical point*.

plementations.¹³ We generate 4×10^5 random points uniformly distributed within the fundamental domain of the moduli space (see Figure 1), scanning over the discrete parameters n_1, n_2, m_1, m_2 . The initial values for our implemented search lie within the ranges

$$\begin{aligned}
 -0.6 \leq \text{Re}(\tau) \leq 0.6, & & \sqrt{1 - (\text{Re} \tau)^2} \leq \text{Im}(\tau) \leq 1.3, \\
 0.5 \leq \text{Re}(S) \leq 2.0, & & -1 \leq \text{Im}(S) \leq 1.
 \end{aligned}$$

As mentioned earlier, instead of focusing only on local minima, our search aims to locate as

¹³`PyTorch` can be customised to minimise the potential; however, despite its high speed, it typically converges to minima where the dilaton runs away. Exploring improved versions is left for future work.

many critical points of the scalar potential in Equation (36) as possible. For each sampled point, we compute ∇V and use `FindRoot` to solve for critical configurations. Numerical convergence was established by requiring $|\nabla V| \lesssim 10^{-20}$ for all critical points. If ∇V fails to vanish within tolerance (or any numerical issues arise during evaluation), the point is classified as *Not a critical point*.

After identifying the critical points, they are then tested against runaway behaviour in the dilaton, signalled by divergent values of $\text{Re}(S)$, as they indicate a negligible gauge coupling and an undesirably unstable modulus.

To assess the stability of the critical points with a finite value of $\text{Re}(S)$, we evaluate the eigenvalues of the Hessian $\nabla^i \nabla_j V$. Configurations with all positive eigenvalues are labelled as (locally stable) *Vacuum*, while those with one or more negative eigenvalues are classified according to the number and orientation of the tachyonic directions. In particular, we distinguish between solutions with a single tachyonic mode (often indicating a mild instability) and those with multiple tachyons.

The analysis is further refined by determining whether the dominant instability aligns with $\text{Re}(S)$, which dictates the gauge coupling. Configurations exhibiting this behaviour are labelled *Tachyonic gauge coupling*, reflecting an instability in the gauge sector during field evolution. Similarly, solutions where the instability combines the axions $\text{Re}(\tau)$ and $\text{Im}(S)$ are grouped as *Tachyonic axion*. Those with multiple unstable directions are placed in the *Many tachyons* category.

Figure 4 summarises the distribution of the values of the real components of the moduli and the integer parameters n_a, m_a of Equation (29). The radial chart displays the Z-score of each variable for a better comparison. The zero Z-score, described by the second dashed circular contour from the center and marked with a 0, corresponds to the mean values of the variables. Further contours differ by a σ deviation from the mean values. Both the mean and the deviation are given in the table of that figure. This provides a compact comparative view of the structure associated with all classes. Note that the green polygon, which indicates unstable one-dimensional saddles of V , includes mostly average values for m_1 while the parameters n_1, n_2, m_2 are off by about 1σ from their statistical mean in our search; furthermore, this polygon shows that e.g. the VEV of the real component of the dilaton (and hence the gauge coupling) is average while $\langle \text{Re}(\tau) \rangle$ is well below average.

Further, the resulting distributions of the various classes are shown in the complex planes of τ and S in Figures 5 and 6, respectively, where the marker shape and colour denote the class, and opacity is adjusted to highlight vacuum and tachyonic gauge coupling classes. Concerning the possible presence of modularly equivalent points in the numerical results, we carried out an explicit verification for modular redundancies. While search seeds were

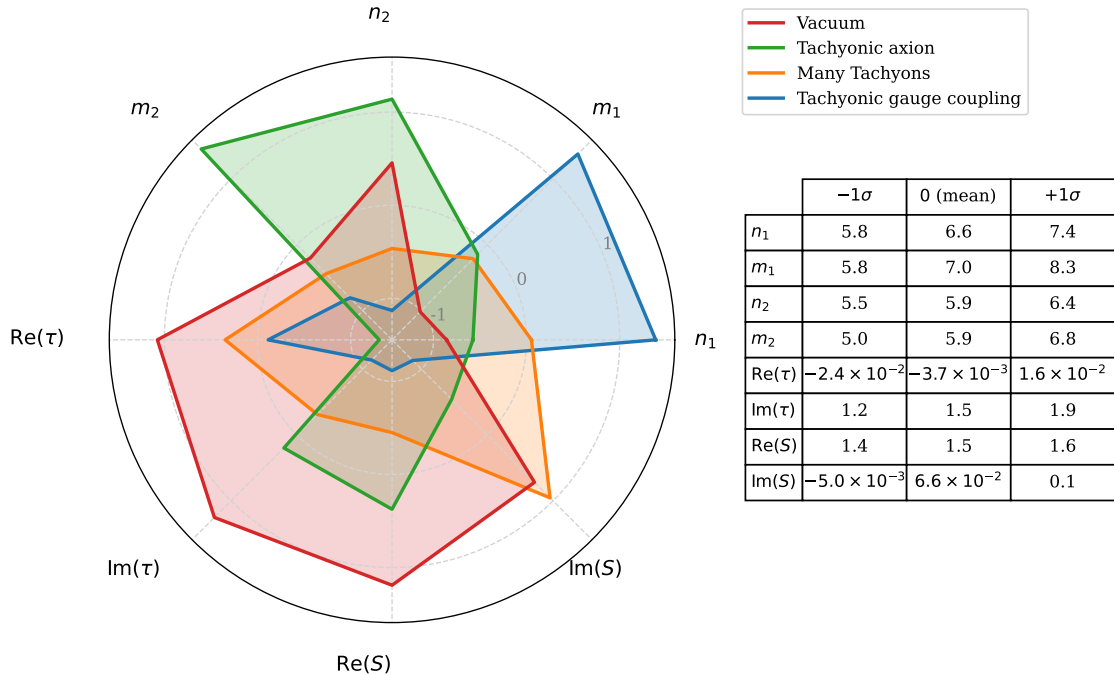


Figure 4: Z-score radar chart of the parameter and moduli values for the different classes of solutions. Each polygon compares how the Z-scores of the various parameters and moduli distribute, based on their mean values and σ variance to facilitate direct comparison. The innermost (outermost) circle corresponds to the mean value minus (plus) 1σ for all variables. The table provides these statistical values for each variable in our search. The unphysical classes *Not a critical point* and *Gauge runaway* are omitted.

drawn from the fundamental domain, we performed an *a posteriori* verification to ensure the final dataset is free of modular redundancies. Equivalent solutions identified via the $\text{SL}(2, \mathbb{Z})$ mapping (including the Green-Schwarz transformation) constituted a negligible subset ($< 0.01\%$) and were subsequently removed. A striking feature emerges in Figure 5: solutions in the *Tachyonic axion* class cluster in angular regions forming a distinctive “penacho”¹⁴ pattern in the τ -plane. The significance of this plume-like structure remains unclear, though it may suggest deeper constraints imposed by modular invariance. Further investigation is needed to determine its potential relevance. Stable vacua appear more sparsely, typically near the boundaries of the fundamental domain. While *Not a critical point* outcomes appear to occupy complementary regions, this effect is not statistically

¹⁴The name “penacho” is a nod to the famed feathered headdress of Moctezuma, currently held in Vienna; it is a cultural reminder that what is displaced can still speak meaningfully to its origins.

significant.

Figure 6 shows the distribution of the classes described in Figure 3 in the dilaton plane. The solutions cluster within the initial search range, $\text{Re}(S) \in (0.5, 2.0)$, as expected. However, additional physically relevant solutions are found outside this region, favouring the weaker coupling regime ($\text{Re}(S) > 2.0$) over the stronger coupling limit ($\text{Re}(S) < 0.5$). Notably, the *Tachyonic gauge coupling* class exhibits periodic alignment in horizontal bands, reflecting the axionic character of $\text{Im}(S)$. In contrast, the *Vacuum* and *Tachyonic axion* classes do not display such periodicity. A vertical band with a comparatively low density of solutions appears near $\text{Re}(S) = 1.5$, a feature that warrants further investigation. As expected, the *Not a critical point* class is distributed broadly across the entire complex plane.

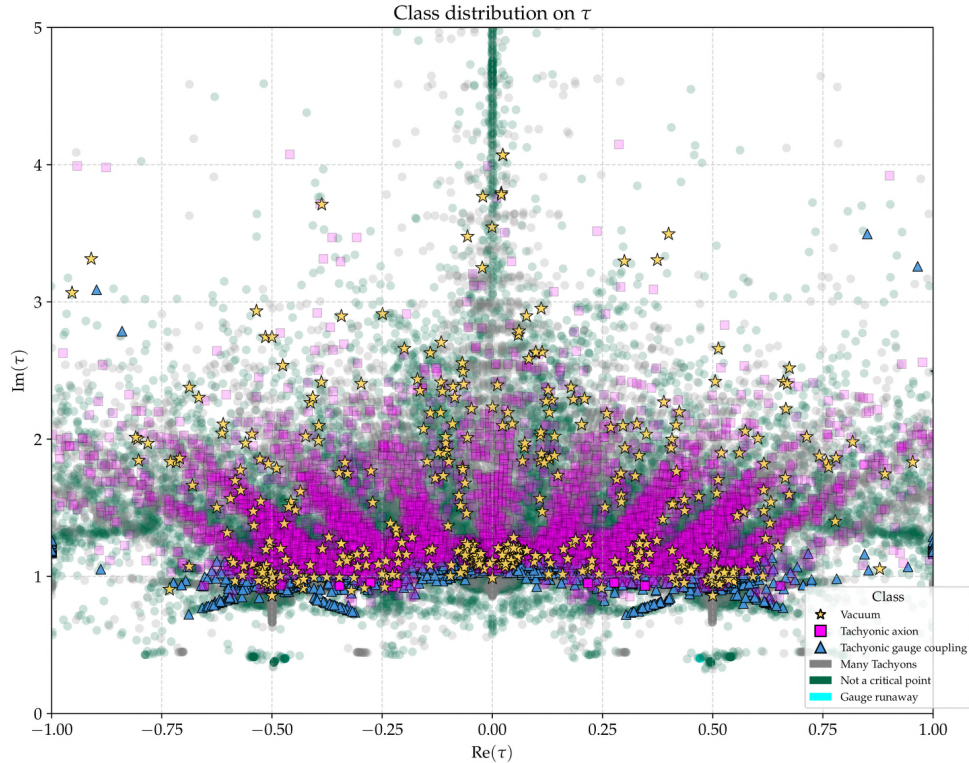


Figure 5: Distribution of the classes from Figure 3 in the complex τ -plane. Solutions corresponding to stable vacua are represented by yellow stars, whereas those identified as *Tachyonic axion* are marked with pink squares. *Tachyonic gauge coupling* solutions are represented with blue triangles, while different colours distinguish the remaining cases. Solutions classified as *Tachyonic axion* cluster in specific angular regions with a “penacho”-like structure, while the apparent tendency of the *Not a critical point* class to occupy complementary sectors is not statistically robust. Stable vacua occur more often near the boundaries of the fundamental domain, though they also appear sporadically throughout the region without a dominant spatial pattern.

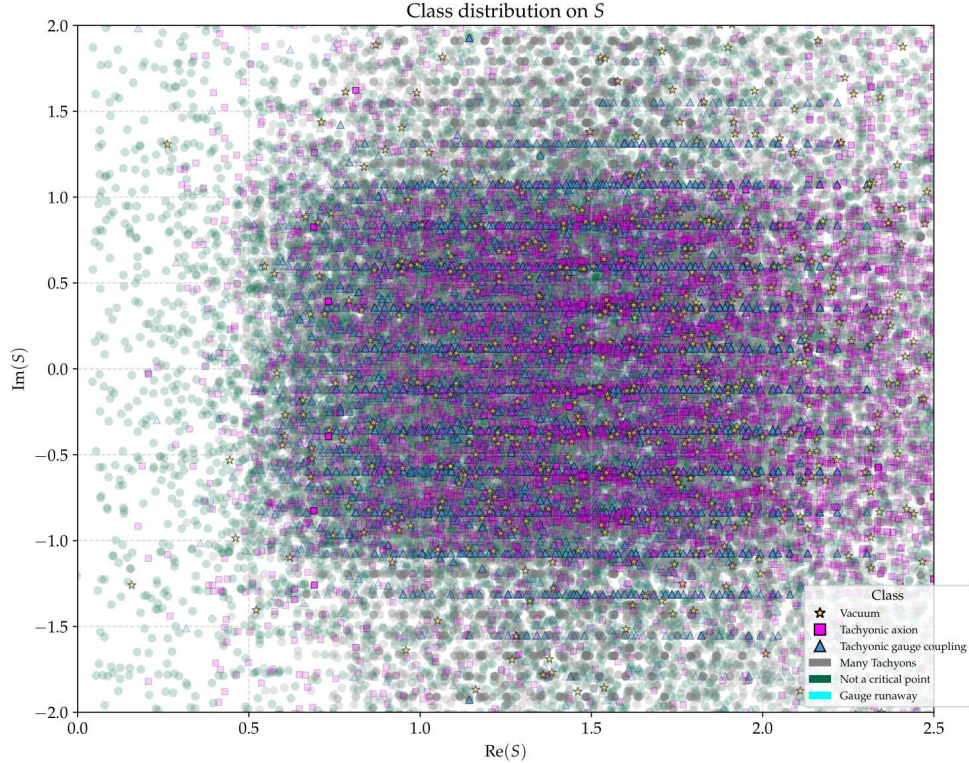


Figure 6: Distribution of the classes from Figure 3 in the dilaton plane. Solutions corresponding to stable vacua are represented by yellow stars, whereas those identified as *Tachyonic axion* are marked with pink squares. *Tachyonic gauge coupling* solutions are represented with blue triangles, while different colours distinguish the remaining cases. Solutions in the *Tachyonic axion* class do not exhibit a clear spatial pattern, although they are more frequently located within the range $\text{Im}(S) \in [-1, 1]$. Solutions classified as *Vacuum* are dispersed without a dominant distribution trend. Notably, *Tachyonic gauge coupling* solutions tend to align periodically along horizontal bands at specific values of $\text{Im}(S)$.

3.1 Properties of the critical points

Until now, we have analysed the structure and distribution of the critical points of the potential according to the classification scheme of Figure 3. Here we highlight several properties of these solutions that are relevant to the swampland programme [9, 10] and will be important for our cosmological analysis in the next section.

3.1.1 Supersymmetry of adS minima

An immediate question is whether supersymmetry is preserved in the adS minima we find.¹⁵ To address this, we compute the F -terms, proportional to $D_\Phi W$, along with the value of the superpotential W at each minimum. For all minima, we find

$$\langle D_\tau W \rangle \sim \mathcal{O}(10^{-19}), \quad \langle D_S W \rangle \sim \mathcal{O}(10^{-20}), \quad \langle W \rangle \sim \mathcal{O}(10^{-5}). \quad (37)$$

Moreover, the ratio between the first term in Equation (34), $K^{A\bar{B}} D_A W D_{\bar{B}} \bar{W}$, and the second term, $3|W|^2$, is always $\lesssim \mathcal{O}(10^{-23})$. This indicates that all adS minima we find are supersymmetric, at least to the precision of our numerical search.

3.1.2 Unstable dS

Consistent with previous studies in heterotic orbifolds [7], we do not find any dS minima. However, we do identify a large number of dS saddle points. As first noted in [11], such saddles can support thawing quintessence scenarios, in which scalar fields roll slowly from an initially frozen state (see [41] for cosmological constraints on the single-field saxion case, and other string-motivated hilltop constructions). This possibility is particularly interesting in view of recent cosmological results [29–35], which hint at a DDE component rather than a pure cosmological constant. In the next section, we focus on the class of *Tachyonic axion* saddle points, which arise naturally in our modular-invariant heterotic potential and can drive multifield hilltop quintessence.

3.1.3 Impact of modular invariance.

To conclude this subsection, we investigate whether modular symmetry plays an essential role in our results. To this end, we explicitly break modular invariance in the potential¹⁶ and repeat our search. We find that the appearance of *tachyonic axion* saddle points is strongly suppressed: out of 10^5 candidate critical points, only eight such saddles occur without modular invariance, compared to 970 in the modular-invariant case. This striking difference suggests that modular symmetry is not merely a consistency requirement, but actively shapes the vacuum structure and the presence of cosmologically relevant saddles.

¹⁵Our model also presents adS critical points exhibiting (one or more) tachyonic directions.

¹⁶To this end, we modified the non-perturbative contribution to the superpotential (28) as $W_{\text{gc}} = \Omega_1(S)H_1(\tau) + \Omega_2(S)H_2(\tau)$. In this way, the superpotential (35) does not transform as a modular form with modular weight -1 , breaking modular invariance.

3.2 Tests on swampland conjectures

The swampland program seeks to identify the criteria that an effective field theory (EFT) must fulfill in order to admit a consistent ultraviolet (UV) completion within a theory of quantum gravity. These criteria are encapsulated in various swampland conjectures (see e.g. [9, 10] for recent reviews), which aim to delineate the landscape of viable low-energy theories from the vast space of inconsistent, or swampland, models.

Although our current setup is a string-inspired heterotic orbifold compactification, based on the important principle of modular invariance which governs the scalar potential, it is both natural and insightful to examine the compatibility of our model with various swampland conjectures. This section is devoted to precisely that analysis.

3.2.1 Refined dS conjecture

We begin with the refined dS conjecture [12, 13] introduced in the introduction. The conjecture asserts that the scalar potential V in any EFT consistent with quantum gravity must satisfy at least one of the conditions in Equation (1), reproduced here for convenience:

$$\sqrt{\nabla^j V \nabla_j V} \geq c V \quad \text{or} \quad \min(\nabla^i \nabla_j V) \leq -c' V, \quad (38)$$

where c and c' are positive constants of $\mathcal{O}(1)$, and $\min(\nabla^i \nabla_j V)$ denotes the smallest eigenvalue of the field-space covariant mass matrix $\nabla^i \nabla_j V$.

Interestingly, the unstable dS vacua we identify do not satisfy the gradient bound, and therefore we focus on the second condition. Specifically, we evaluate the ratio

$$r := \frac{\min(\nabla^i \nabla_j V)}{V} \quad (39)$$

to verify whether it meets the required threshold. Our analysis shows that all unstable dS vacua in our model satisfy this bound, with values reaching as low as $r \lesssim -11$.

These results are consistent with previous analysis on heterotic orbifolds of [7, 11] and [55], where it was argued that metastable dS vacua can only emerge upon incorporating stringy corrections (such as Shenker-like effects [110]) into the Kähler potential. In their absence, no metastable dS vacuum is viable, as it is the case in our framework.

3.2.2 AdS scale separation

As discussed above, the adS minima we obtain are all supersymmetric to the numerical precision specified earlier. Although our cosmological analysis in the next section will focus

on unstable dS saddles, the adS vacua remain relevant: they act as the late-time end points of the rolling trajectories we find, and their properties determine the ultimate fate of the evolution.

A particularly interesting property to examine is whether these adS vacua exhibit *scale separation*, namely a clear hierarchy between the Kaluza–Klein scale L_{KK} and the adS curvature radius L_{AdS} ,

$$\frac{L_{\text{KK}}}{L_{\text{AdS}}} \ll 1, \quad (40)$$

which would support the validity of a lower-dimensional effective description. This question has gained renewed attention in light of recent conjectures on the absence of *parametric* scale separation in string theory [111,112], although here we do not seek a parametric limit. Our analysis is instead in the spirit of studies of individual scale-separated vacua, as in e.g. [113,114] (see [115] for a review of the parametric conjecture and [116–119] for recent related work).

We define L_{AdS} in terms of the cosmological constant as $\Lambda = -3/L_{\text{AdS}}^2$, and take L_{KK} from the standard heterotic estimate for the Kaluza–Klein mass scale,

$$\Lambda_{\text{KK}} = 18\sqrt{k}, \quad (41)$$

with k the Kač–Moody algebra level [120].

For a statistical test, we analyse 744 adS vacua obtained from non-equivalent models with distinct choices of the discrete parameters (n_1, n_2, m_1, m_2) . We find that *all* vacua satisfy

$$\frac{L_{\text{KK}}}{L_{\text{AdS}}} < 10^{-3}, \quad (42)$$

comfortably within the bound (40). This indicates that the adS vacua in our heterotic orbifold set-up admit a well-controlled 4D effective description.

4 Multifield quintessence from modular dS saddles

We have seen that the modular invariant potential (36) exhibits a rich landscape of dS saddle points, all consistent with the refined de Sitter swampland conjecture (1). At the same time, recent cosmological observations hint at an evolving dark energy equation of state. Within quintessence scenarios, the data appear to favour *thawing* models, where the equation of state w_φ begins close to -1 and gradually increases. Hilltop quintessence [121] provides a well-studied realisation of this class and has been explored in supergravity and string-motivated settings [11]. More recently, single-field axion and saxion hilltops have been directly confronted with the DESI and DES data in [41].

Motivated by this, we now investigate cosmological evolution in the modular invariant heterotic potentials introduced above. In particular, we study the dynamics near a dS saddle point in the full four-field system of the complex dilaton S and Kähler modulus τ . This extends earlier single-field hilltop constructions to a setting where multiple moduli can roll simultaneously, as is generically expected in string compactifications.

Concretely, we focus on a representative saddle point with a single tachyonic direction dominated by the dilaton axion:

$$\text{Im}(\psi^S) \sim 0.9 \text{Im}(S) - 0.4 \text{Re}(\tau), \quad (43)$$

belonging to the *Tachyonic axion* branch of our classification in Section 3 (see Figure 3). Starting from this configuration, we evolve the fields along their cosmological trajectory as they roll towards a nearby adS minimum. The parameter values and vacuum expectation values at the saddle are listed in Table 3.

The dynamics are governed by the coupled Einstein–scalar system:

$$3 \left(\frac{\dot{a}}{a} \right)^2 = \frac{1}{2} g_{ij} \dot{\varphi}^i \dot{\varphi}^j + V + 3H_0^2 \Omega_{M,0} a^{-3} + 3H_0^2 \Omega_{r,0} a^{-4}, \quad (44a)$$

$$0 = \ddot{\varphi}^i + 3 \frac{\dot{a}}{a} \dot{\varphi}^i + \Gamma_{jk}^i \dot{\varphi}^j \dot{\varphi}^k + g^{ij} \partial_j V, \quad (44b)$$

where we assume a flat Friedmann–Lemaître–Robertson–Walker (FLRW) metric with scale factor $a(t)$ and we include matter and radiation, whose contributions are encoded in the density parameters today,

$$\Omega_{i,0} := \frac{\rho_{i,0}}{3H_0^2}, \quad \text{with} \quad \rho_i \propto a^{-3(1+w_i)} \quad (45)$$

and w_i the equation of state of each component. The scalar fields are denoted together as

$$\varphi = (\varphi^i) = (\text{Re}(\tau), \text{Im}(\tau), \text{Re}(S), \text{Im}(S)), \quad (46)$$

with field-space metric

$$\frac{\partial^2 K}{\partial \Psi^I \partial \bar{\Psi}^J} \partial \Psi^I \partial \bar{\Psi}^J = \frac{1}{2} g_{ij} \partial \varphi^i \partial \varphi^j, \quad (47)$$

for $\Psi^I = \{\tau, S\}$. The scalar potential V is given in Equation (36). We stress that in our analysis we incorporate one-loop corrections, which appear both in the scalar potential and in the Kähler metric. These corrections are crucial for a consistent heterotic orbifold description and imply that the field-space metric is no longer diagonal. In fact, at the saddle point under consideration, the corrected metric takes the form

$$g_{1\text{-loop}} = \begin{pmatrix} 0.298 & 0 & 0 & -0.00125 \\ 0 & 0.298 & 0.00125 & 0 \\ 0 & 0.00125 & 0.256 & 0 \\ -0.00125 & 0 & 0 & 0.256 \end{pmatrix}, \quad (48)$$

Parameters		
$\tilde{\lambda}_1 = 3/25000, \tilde{\lambda}_2 = 3/5000000$	$m_1 = 12, n_1 = 0, m_2 = 10, n_2 = 3$	$b_1^0 = -9, b_2^0 = -12, A = 6.70 \times 10^{-112}$
Moduli VEVs		
Ψ^I	$\text{Re}\langle\Psi^I\rangle$	$\text{Im}\langle\Psi^I\rangle$
τ	-0.004063	1.297
S	1.390	0.1272
Mass eigenstates		
$\psi^I \sim \Psi^I$	$m_{\text{Re}(\psi^I)}^2$	$m_{\text{Im}(\psi^I)}^2$
ψ^τ	3.190×10^{-116}	3.292×10^{-116}
ψ^S	2.830×10^{-119}	-3.574×10^{-119}
<i>Tachyon:</i> $\text{Im}(\psi^S) \sim -0.4 \text{Re}(\tau) + 0.9 \text{Im}(S)$		

Table 3: Axionic saddle point of the potential (36). The values of m^2 correspond to the eigenvalues of the mass matrix $\nabla^i \nabla_j V$. The mass eigenstate ψ^I has a dominant contribution of the modulus Ψ^I . The unstable direction is mostly governed by the axionic fields $\text{Re}(\tau)$ and $\text{Im}(S)$. All VEVs and masses are given in reduced Planck units with $M_{\text{Pl}} = 1$.

to be contrasted with the tree-level result, which is purely diagonal.

To match the present-day universe, we impose that the cosmological evolution reproduces the observed density fractions and the effective equation of state today. Although these quantities are somewhat model-dependent, significant deviations from the Λ CDM values are not expected. As fiducial values, we adopt those reported by Planck [122]:

$$\Omega_{m,0} = 0.3111, \quad \Omega_{r,0} = 0.0001, \quad \Omega_{\varphi,0} = 0.6889, \quad (49)$$

as well as $H_0 = 5.927 \times 10^{-61}$.

We solve the equations of motion (44) numerically, using the number of e-folds $N = \ln a$ as the evolution variable instead of cosmic time. As is well known in hilltop-like quintessence, if the fields start exactly at the saddle point, they remain there throughout the entire cosmological history, with the potential energy contributing as a cosmological constant. For DDE to arise, however, the fields must be slightly displaced from the saddle, after which they begin to roll down their potential.

Accordingly, we start the fields with a small displacement from the saddle point,

$$\varphi_{\text{init}}^i = \langle\varphi_{\text{saddle}}^i\rangle + \delta\varphi^i, \quad (50)$$

with $\delta\varphi = (-0.00025, 0.0001, 0.0001, -0.0001)$, where φ is defined in Equation (46). The

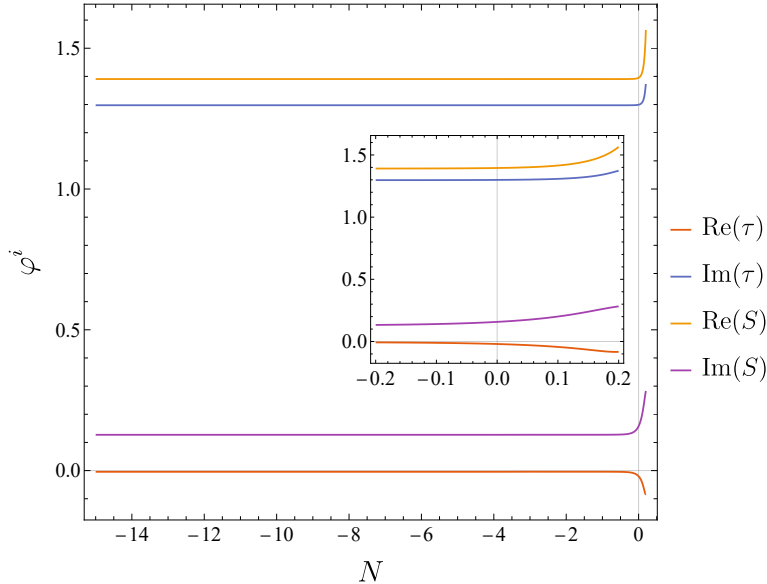


Figure 7: Evolution of the fields φ^i as function of the number of e-folds N . These curves represent the numerical solutions to the equations of motion (44), using the parameters listed in Table 3. The initial conditions are slightly displaced from the saddle point by $\delta\varphi = (-0.00025, 0.0001, 0.0001, -0.0001)$. Here, $N = -15$ corresponds to some time between BBN and matter-radiation-equality, while $N = 0$ represents the present time.

initial conditions must be extremely close to the saddle in order to prevent the energy density from becoming negative before the present epoch, which would otherwise trigger a rapid recollapse. In fact, ensuring that the quintessence equation of state satisfies $w_\varphi < -1/3$ to the present day requires $\delta\varphi^i \lesssim 10^{-3}$. In addition, the potential value at the saddle point must be fine-tuned, as is generic in quintessence scenarios. Here we rescale the potential by an overall factor,

$$\tilde{V} = AV, \quad A = 6.7 \times 10^{-112}, \quad (51)$$

so as to reproduce the observed small value of dark energy today. This rescaling may be related to the VEVs of matter fields and to the polynomials $P(j(\tau))$ associated with gaugino condensates in Equation (29).

The evolution of the four real scalar fields is displayed in Figure 7. We take $N = -15$, which corresponds to an epoch between big bang nucleosynthesis (BBN) and matter-radiation equality (the latter occurring at $N \simeq -8.1$), while matter-dark energy equality happens around $N \simeq -0.26$, and $N = 0$ denotes the present time. The integration is continued until $N \simeq 0.2$ (about 3.0×10^9 years into the future¹⁷) to capture the full

¹⁷One e-fold today corresponds to roughly 14.5 Gyr, hence 0.2 e-folds correspond to ~ 3 Gyr.

trajectory of the fields after they drive cosmic acceleration.

As shown, all four fields remain frozen for most of the cosmological history and only begin to roll very recently, thereby driving the present accelerated expansion. The Kähler modulus is stabilised at $\tau \simeq i$ up to the present epoch, a point that has been extensively studied in flavour phenomenology, where it leads to realistic fermion mass hierarchies [123, 124]. Meanwhile, the real part of the dilaton is stabilised at $\text{Re}(S) \simeq 1.390$, yielding the universal 4-dimensional gauge coupling

$$g_4^2 = \frac{1}{\text{Re}\langle S \rangle} \simeq 0.719. \quad (52)$$

This value is of order unity, consistent with the expectation that the effective gauge couplings in heterotic orbifolds should be moderately strong, lying near the edge of the perturbative regime where control is still maintained. Finally, we note that in the far future the fields evolve towards a nearby adS minimum, as will be discussed in Section 4.2.

Figure 8 shows the evolution of the quintessence equation of state w_φ and the density fractions Ω_i . As expected, the fields roll extremely slowly until very recently, keeping $w \simeq -1$ for most of cosmological history. At present, we find in our model

$$w_{\varphi,0}^{\text{mod}} \simeq -0.9877 \quad \text{and} \quad \Omega_{\varphi,0}^{\text{mod}} \simeq 0.6883,$$

in excellent agreement with observations.

Field displacement and the distance conjecture

We can further compute the total geodesic displacement of the scalar fields from $N = -15$ up to today ($N = 0$), obtaining $\Delta\varphi \simeq 0.16$. This value lies safely within the bound imposed by the so-called *distance conjecture*. This conjecture [125] states that in any EFT consistent with quantum gravity, the field space displacement must satisfy

$$\Delta\varphi \lesssim \tilde{c}, \quad (53)$$

with $\tilde{c} \sim \mathcal{O}(1)$. Exceeding this bound would signal the appearance of an infinite tower of states becoming exponentially light,

$$m \sim e^{-\alpha\Delta\varphi}, \quad \alpha \sim \mathcal{O}(1), \quad (54)$$

which invalidates the LEEFT description. This reflects the expectation that large excursions in field space trigger the emergence of new degrees of freedom, signalling the breakdown of the effective description.

It should be emphasised that our computation does not include the very early universe, e.g. possible epochs immediately after inflation. For instance, a kination phase is possible in scalar models, during which $\rho \propto a^{-6}$ and the field displacement could be substantially larger. However, such epochs are highly model dependent and are not guaranteed to occur or last for long in the present setup.

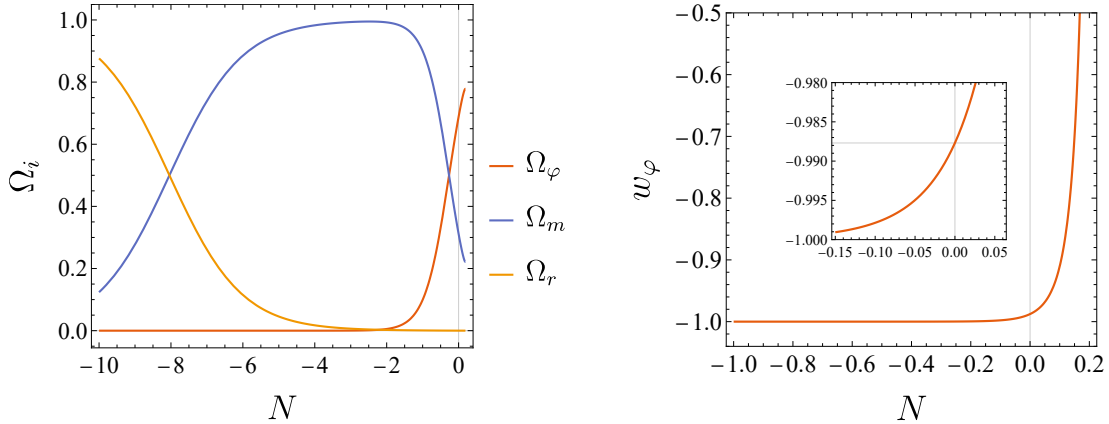


Figure 8: Evolution of the cosmological observables as functions of the number of e-folds N . Their current values are $\Omega_{\varphi,0}^{\text{mod}} \simeq 0.6883$, $\Omega_{m,0}^{\text{mod}} \simeq 0.3116$, $\Omega_{r,0}^{\text{mod}} \simeq 0.0001$ and $w_{\varphi,0}^{\text{mod}} \simeq -0.9877$.

4.1 Cosmological constraints on w_φ

Although we do not perform a full likelihood analysis against cosmological data, we can nevertheless confront our background evolution with observational constraints, in particular on the dark energy equation of state. We focus on the most recent DESI-DR2 results, which report constraints on w_{DE} based on the commonly used Chevallier-Polarski-Linder (CPL) parametrisation [126, 127], where the dark energy equation of state is expressed as

$$w_{\text{DE}}(a) = w_0 + (1 - a) w_a, \quad (55)$$

namely a first-order Taylor expansion of w_{DE} in the scale factor a , with linear leading behaviour. Considering the combined DESI+CMB+Union3 datasets [32], the reported constraints are

$$w_0 = -0.667 \pm 0.088 \quad \text{and} \quad w_a = -1.09_{-0.27}^{+0.31}. \quad (56)$$

While our saddle quintessence model is not expected to be captured by the CPL ansatz, it is still instructive to compare. We find that by slightly adjusting the initial displacement

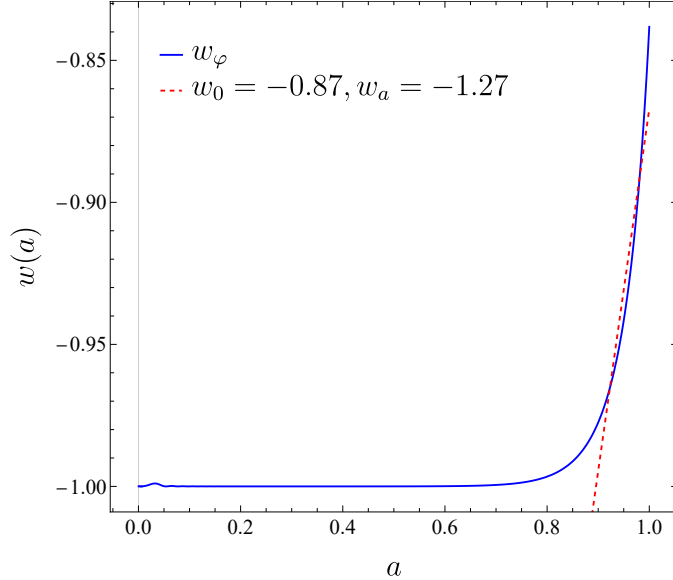


Figure 9: Equation of state parameter w as a function of the scale factor a for our quintessence model φ , compared with the CPL parametrization of DESI [32]. The linear fit was performed between $a = 0.9$ and $a = 1.0$. The red dashed line yields a chi-squared error of $\chi^2 \simeq 5.6$, where we have compared with DESI+CMB+Union3 data.

from the saddle point, one can obtain values of w_0 closer to those in (56). For instance, displacing the fields as

$$\delta\varphi = (0.000641, 0.0001, 0.0001, 0.000185), \quad (57)$$

yields a present-day value $w_0 = -0.838$. Larger values of w_0 closer to -1 , or significantly higher values, can be obtained similarly with suitable initial conditions. This sensitivity is in fact a well-known feature of hilltop quintessence: the evolution of w_φ is highly dependent on both the displacement from the maximum and the local curvature of the potential [121]. We find that for displacements $\delta\varphi_{\max}^i \gtrsim 10^{-3}$, the fields are too far from the saddle and roll too fast to remain compatible with acceleration today.

In Figure 9 we show the comparison between the CPL parametrisation and our saddle quintessence evolution. The CPL parameters were obtained by fitting the model’s approximately linear behaviour in the interval $a = 0.9$ to $a = 1$. When compared with the DESI+CMB+Union3 results, our fit yields a best-fit deviation corresponding to $\chi^2 \simeq 5.6$.

A more accurate parametrisation for single-field hilltop quintessence was obtained by Dutta–Scherrer [121] and extended to general thawing models by Chiba [128] (DSCh). This parametrisation was obtained considering an expansion around the maximum (initial value of ϕ in [128]) of the potential $V(\phi) = V(\phi_{\max}) + V''(\phi_{\max})(\phi - \phi_{\max})^2$. However,

since our scenario involves four coupled scalar fields, this assumption cannot be made and thus a large discrepancy will arise. Developing an accurate parametrisation for multifield saddle quintessence thus remains an interesting task for future work.

4.2 The fate of dark energy: descent into adS

Thus far we have focused on the multifield dynamics relevant for today’s universe. It is, however, interesting to let the fields evolve further in the future to determine the fate of today’s accelerated expansion in the class of models we study. In particular, in the saxion supergravity hilltop of [11,41], the late-time dynamics drive the system towards a runaway at large field values. Since the potential in that case is unbounded from below at small saxion values, an additional fine-tuning was required to ensure that the field started slightly displaced from the hilltop, rolling towards larger values. In contrast, in the present setup we can displace the fields from the saddle either towards smaller or larger values of the four scalars. This allows us to track the full evolution of the system and determine, without additional tuning, the eventual fate of dark energy in our model.

Remarkably, as already noted, the fields evolve towards one of the adS minima of the full potential. This implies that the current accelerated expansion is only a *transient* phenomenon. To numerically study the complete trajectory, we uplift the potential by a constant term such that the minimum is shifted to zero, ensuring positivity of the potential throughout the evolution:

$$V_{\text{up}} = V + \varepsilon, \tag{58}$$

with $\varepsilon = 9.397 \times 10^{-122}$. Evolving the system with this uplift, we observe the fields rolling towards the nearby adS minimum, oscillating around it as shown in the left panel of Figure 10¹⁸. From the numerical solution we extract the precise location of the minimum, its potential value, and the Hessian eigenvalues, summarised in Table 4. The right panel of Figure 10 illustrates the full trajectory of the Kähler modulus, with the adS vacuum located at $\tau = -0.1650 + 1.385i$, lying within the fundamental domain.

As discussed in Section 3.1.1, all adS minima we identify are supersymmetric up to numerical precision. At the endpoint minimum reached dynamically, we compute the F -terms, proportional to $D_{\Psi}W$, as well as the superpotential W (before including the constant

¹⁸See e.g. [129–132] for cosmological constraints on models with a negative cosmological constant.

A). Our results read

$$\begin{aligned}
\langle D_\tau W \rangle &= 1.24 \times 10^{-19} - 5.25 \times 10^{-20} i, \\
\langle D_S W \rangle &= -6.10 \times 10^{-20} - 4.28 \times 10^{-20} i, \\
\langle W \rangle &= 2.04 \times 10^{-5} - 7.02 \times 10^{-6} i.
\end{aligned}
\tag{59}$$

Moreover, the ratio between the first and second terms in Equation (34), $K^{A\bar{B}} D_A W D_{\bar{B}} \bar{W}$ and $3|W|^2$, is 1.30×10^{-28} , again confirming supersymmetry to numerical accuracy.

At first glance, the fact that the system evolves towards a vacuum rather than a runaway, as in [11,41], may seem surprising. However, this behaviour can be understood from the structure of the potential. Indeed, only $\text{Re}(S)$ admits a genuine runaway. The axionic components, $\text{Re}(\tau)$ and $\text{Im}(S)$, are stabilized by the expected periodic potentials, while V diverges as $\text{Im}(\tau) \rightarrow \infty$. Although the $\text{Re}(S)$ direction exhibits a runaway behaviour, the dilaton initially sits at a local minimum and, throughout the entire cosmological evolution, it closely follows this minimum. We illustrate the dynamics of $\text{Re}(S)$ explicitly in Figure 11.

In summary, in the class of models we discuss, the present accelerated expansion is not eternal: the universe is ultimately destined to settle into a supersymmetric adS vacuum.

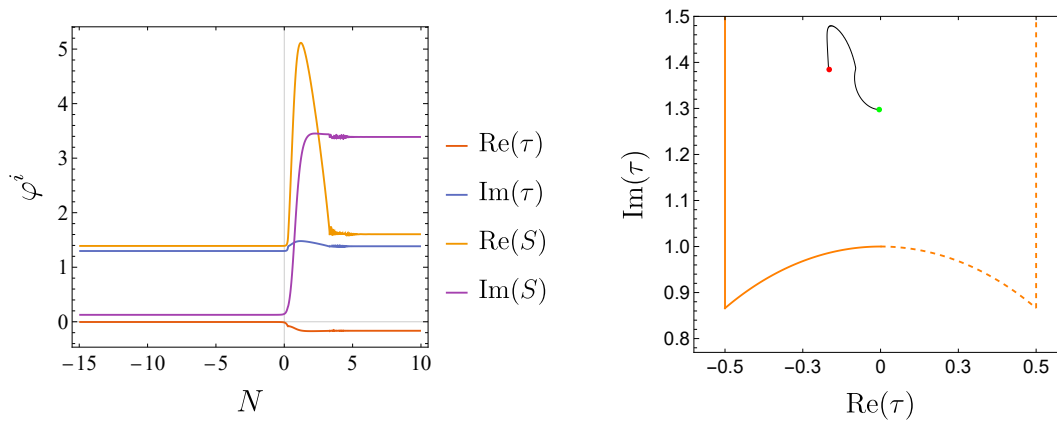


Figure 10: Evolution of the fields φ_i . The left panel shows the values of the fields as a function of the number of e-folds N . The right panel presents the parametric plot of the Kähler modulus τ . The green dot marks the saddle point, while the red dot represents the adS minimum. It can be observed that the fields oscillate around the minimum until they stabilise.

Moduli VEVs		
Ψ^I	$\text{Re} \langle \Psi^I \rangle$	$\text{Im} \langle \Psi^I \rangle$
τ	-0.1650	1.385
S	1.605	3.389
Mass eigenstates		
$\psi^I \sim \Psi^I$	$m_{\text{Re}(\psi^I)}^2$	$m_{\text{Im}(\psi^I)}^2$
ψ^τ	1.925×10^{-116}	1.920×10^{-116}
ψ^S	5.292×10^{-118}	5.206×10^{-118}
Potential value: $V = -1.052 \times 10^{-121}$		

Table 4: AdS minimum of the potential. With the uplift in Equation (58), the fields evolve until reaching this stable vacuum.

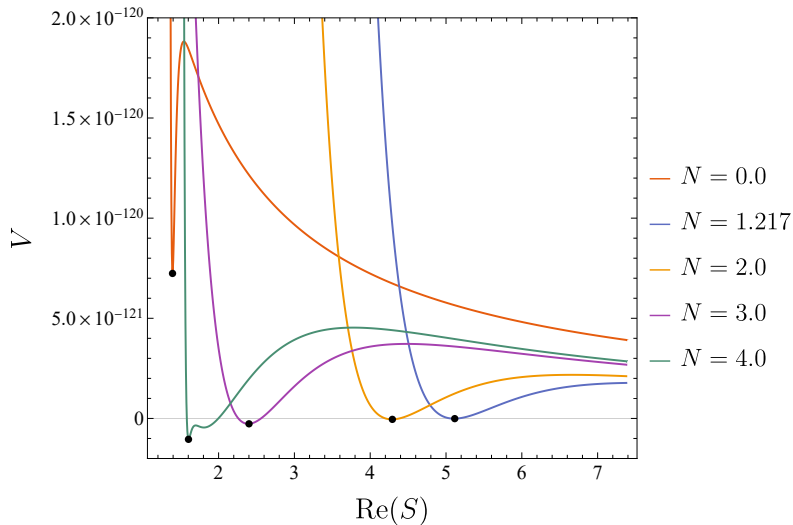


Figure 11: Scalar potential V as a function of $\text{Re}(S)$ for different e-fold values N . The black dots indicate the evolution of $\text{Re}(S)$ as N increases, from dS at $N = 0$ (today) to adS at $N = 4$ (distant future). The field remains consistently at a local minimum along this direction throughout its evolution.

5 Discussion and Outlook

Heterotic orbifolds are among the simplest string constructions that can reproduce many features of particle physics, thanks to their rich symmetry structure. In particular, modular symmetries naturally appear in these models as inherited from the toroidal structure of the compact space. Such symmetries have recently attracted wide attention both in the context of flavour physics, where they serve as instrumental restrictions to reach predictions, and

in the swampland program, where they provide a guiding principle for formulating quantum gravity constraints. Thus, heterotic orbifolds provide a natural arena for connecting particle phenomenology, swampland constraints, and cosmological dynamics.

In this work, we have shown that heterotic orbifolds combine these ingredients into a coherent framework. As a working example, we studied a two-dimensional $\mathbb{T}^2/\mathbb{Z}_3$ orbifold sector of a heterotic orbifold compactification without Wilson lines. In this case, the $SL(2, \mathbb{Z})$ modular symmetry governing the dynamics of the toroidal modulus τ is realised as a $\Gamma'_3 \cong T'$ finite modular symmetry of the effective action. The coupling strengths among matter superfields are then described by VVMFs, which depend solely on τ and build T' representations. Exotic matter associated with hidden non-Abelian gauge sectors is typically decoupled, but their gaugino condensates contribute modular-invariant terms to the effective action, coupling τ and the dilaton S . Other moduli can be stabilised supersymmetrically, as we assume to be the case. The resulting setup, based on the restrictions of the modular T' and gaugino condensates, drives the dynamics of the lightest complex moduli τ and S , which may control aspects of cosmology.

We first performed in Section 3 a systematic exploration of the critical points of the modular-invariant potential, by varying the integers m_a and n_a in the non-perturbative superpotential. Our extensive numerical search uncovered several interesting features for the structure of these critical points, which we classified according to our scheme outlined in Figure 3:

- No dS (meta)-stable vacua were found, in line with the dS swampland conjecture and previous work [7].
- The solutions fall into two categories: *unstable dS critical points* and *stable and unstable adS vacua*.
- The unstable saddles satisfy the refined dS conjecture and exhibit a non-trivial structure in their tachyonic directions, including an interesting “penacho” distribution along axionic directions shown in Figure 5 and distinctive patterns in the dilaton plane as shown in Figure 6. These may simply be coincidences, but determining their relevance requires further study.

We then studied the cosmological implications of this setup in Section 4. These are twofold. First, unstable dS saddles provide natural realisations of multifield hilltop quintessence models, which satisfy swampland constraints. In particular, we showed that axionic combinations of the moduli can drive slow-roll dynamics compatible with the recent observations hinting at a dynamical form of dark energy. Our explicit example yields

an equation-of-state evolution consistent with DESI within 3σ . This suggests heterotic orbifolds as concrete string-based realisations of quintessence, while satisfying swampland constraints. Of course, a full cosmological analysis, including perturbations and couplings to matter, remains to be performed. We stress that this framework does not eliminate the well-known challenges of quintessence, such as fine-tuning, fifth-force bounds, variations of fundamental constants, and the cosmological constant problem itself. For example, as shown in Table 4, the saxion turns out to be very light, which could potentially lead to conflicts with fifth-force constraints, a question that merits further investigation. However, our model provides a natural and UV-complete setting in which these challenges can be systematically addressed.

Second, the stable adS vacua we identified offer further insight into the structure of the landscape. In these solutions, the Kaluza-Klein length scale is generically negligible compared with the adS curvature scale, thereby satisfying the conjecture of scale separation in quantum gravity.

Several avenues remain to be explored and we plan to come back to this in future work. Firstly, a systematic investigation of the “penacho” structure and other statistical patterns in the distribution of tachyonic modes will allow us to determine whether they have a modular or geometric origin. Our setup provides a robust proof of principle, but extending the analysis to include more realistic compactifications with additional moduli and matter fields remains an important next step. Furthermore, exploiting the modular symmetries inherent in heterotic orbifolds to probe quantum gravity conjectures more sharply seems a natural step forward as well. On the cosmological side, it will be interesting to develop a multifield generalisation of the DSCh hilltop parametrisation of the equation of state, enabling a broader comparison between string-based quintessence and data. Furthermore, although we have studied here a model displaying thawing-like behaviour, where the equation of state w_{DE} grows from -1 towards larger values, current analyses also hint at a possible crossing of the phantom divide [32, 133], which motivates further research to realise this non-standard quintessence scenario in string constructions. Also, exploring couplings between dark energy and dark matter within this framework, where an effective phantom-like behaviour may arise [134] is left for future work.

Heterotic orbifolds offer a unifying framework in which modular symmetries, swampland conjectures, particle phenomenology, and cosmology intersect. Our results demonstrate that the landscape of extrema is both structured and phenomenologically rich. Rather than being pathologies to avoid, unstable saddles emerge as natural candidates for quintessence within a UV-complete setting, which deserve further study.

Acknowledgments

It is a pleasure to thank Bruno V. Bento and Timm Wrase for useful discussions and Susha Parameswaran for comments on an earlier version of the manuscript. This work was partially supported by UNAM-PAPIIT grants IN113223 and IN117226, and the Marcos Moshinsky Foundation. IZ is partially funded by the STFC grants ST/T000813/1 and ST/X000648/1. For the purpose of open access, the authors have applied a Creative Commons Attribution license to any Author Accepted Manuscript version arising. Research Data Access Statement: No new data were generated for this manuscript.

A A concrete orbifold model

Our model arises from the heterotic string compactified on the orbifold $\mathbb{Z}_6 - \text{II}$. The model is fully specified by its twist v , shift V and Wilson loops A_5 and A_6 given by

$$v = \frac{1}{6}(0, 1, 2, -3), \quad (60a)$$

$$V = \left(-\frac{5}{12}, -\frac{5}{12}, -\frac{5}{12}, -\frac{5}{12}, \frac{1}{12}, \frac{1}{12}, \frac{1}{12}, \frac{1}{12} \right), \left(-\frac{5}{12}, -\frac{1}{4}, -\frac{1}{4}, -\frac{1}{12}, \frac{1}{12}, \frac{1}{12}, \frac{1}{12}, \frac{1}{12} \right), \quad (60b)$$

$$A_5 = \left(-\frac{5}{4}, \frac{3}{4}, \frac{5}{4}, \frac{7}{4}, -\frac{3}{4}, \frac{1}{4}, \frac{3}{4}, \frac{5}{4} \right), \left(-\frac{1}{2}, 1, 1, -\frac{3}{2}, -1, 0, 1, 1 \right), \quad (60c)$$

$$A_6 = \left(-\frac{3}{2}, -\frac{1}{2}, 1, 1, \frac{1}{2}, 0, -\frac{1}{2}, 1 \right), \left(-\frac{1}{4}, \frac{3}{4}, \frac{3}{4}, \frac{5}{4}, -\frac{1}{4}, \frac{7}{4}, \frac{1}{4}, \frac{7}{4} \right). \quad (60d)$$

By using the `Orbifolder` [3], we obtain the unbroken 4-dimensional (4D) gauge group

$$G = \text{SU}(3)_C \times \text{SU}(2)_L \times \text{U}(1)_Y \times \left(\text{SU}(3)^3 \times \text{U}(1)^6 \right)_{\text{hidden}}. \quad (61)$$

We note that the non-Abelian factors $\text{SU}(3)_{\text{hidden}}^3$ of the gauge hidden sector easily give rise to the gaugino condensates in Equation (28). We have explicitly verified the decoupling of $\text{SU}(3)_{\text{hidden}}$ -charged matter states and computed the beta-function coefficients before and after decoupling, b_1 and b_1^0 , as well as δ_{GS} for one of these gauge factors. With this stringy motivation, we have assumed other suitable values for the corresponding coefficients of the second gaugino condensate to favour the structure of the potential.

The $\mathbb{Z}_6 - \text{II}$ (1, 1) orbifold can be factorised as $\mathbb{T}^2/\mathbb{Z}_6 \otimes \mathbb{T}^2/\mathbb{Z}_3 \otimes \mathbb{T}^2/\mathbb{Z}_2$. On the other hand, from Equation (60), we see that only the third torus is equipped with non-trivial Wilson lines. Hence, as discussed in Section 2.1, the finite modular symmetry related to the $\mathbb{T}^2/\mathbb{Z}_2$ orbifold sector is broken, and, for simplicity, we can focus solely on the symmetries and dynamics of the moduli related to the $\mathbb{T}^2/\mathbb{Z}_3$ orbifold sector.

An appealing feature of $\mathbb{T}^2/\mathbb{Z}_3$ is its eclectic flavour symmetry group [48], consisting of a traditional flavour symmetry $\Delta(54)$, a finite modular symmetry T' and a \mathbb{Z}_9^R symmetry,

sector	string state	T' irrep	$\Delta(54)$ irrep	\mathbb{Z}_9^R charge
untwisted	$\Phi^{(0)}$	$\mathbf{1}$	$\mathbf{1}$	0
	$\Phi^{(-1)}$		$\mathbf{1}'$	3
first twisted	$\Phi^{(-2/3)}$	$\mathbf{2}' \oplus \mathbf{1}$	$\mathbf{3}_2$	1
	$\Phi^{(-5/3)}$		$\mathbf{3}_1$	-2
second twisted	$\Phi^{(-1/3)}$	$\mathbf{2}'' \oplus \mathbf{1}$	$\overline{\mathbf{3}}_1$	2
	$\Phi^{(2/3)}$		$\overline{\mathbf{3}}_2$	5
	$\Phi^{(-4/3)}$		$\overline{\mathbf{3}}_2$	-1
	$\Phi^{(5/3)}$		$\overline{\mathbf{3}}_1$	-1

Table 5: Spectrum of the $\mathbb{T}^2/\mathbb{Z}_3$ orbifold by sector and its irreps under the full flavour eclectic symmetry $T' \cup \Delta(54) \cup \mathbb{Z}_9^R$ [46].

emerging from the outer automorphisms of its Narain lattice [46]. A proper discussion of the flavour problem requires considering both traditional and modular flavour symmetries, as they significantly constrain the Kähler potential and superpotential (see [53] for an explicit study of flavour phenomenology with this eclectic structure). The associated matter spectrum, including charges under this group, is summarized in Table 5. The full expression of the Kähler potential, including moduli and matter terms, is then

$$K = -\log \left[S + \overline{S} - \frac{1}{8\pi^2} \delta_{\text{GS}} \log(i\overline{\tau} - i\tau) \right] - \log(i\overline{\tau} - i\tau) + |\Phi_\alpha|^2 (i\overline{\tau} - i\tau)^{n_\alpha}, \quad (62)$$

which transforms covariantly under the modular symmetry, as in Equation (22). In the LEEFT, the last term is suppressed due to the relatively small VEVs of Φ_α associated with the cancellation of the FI-term (see Section 2.1.4). Further, the assumption of a large volume regime and the restriction to negative fractional modular weights contribute to this suppression. The latter restriction is related to the fact that *massless* states with weights $n_\alpha = 2/3, 5/3$ are rather rare in heterotic orbifold compactifications as they exhibit oscillator excitations.

Now we turn our attention to the Yukawa sector of the effective supergravity theory. For the computation of the superpotential we rely on the selection rules [105] among strings in orbifolds, as implemented in the `Orbifolder`. Considering the relevant terms up to order

five in the model presented above, we obtain (see also [52])

$$\begin{aligned}
W_{\text{Yuk}} \supset \lambda \chi_1 \chi_2 \left[-\frac{\hat{Y}_1(\tau)}{\sqrt{2}} (\Phi_{1,3}\Phi_{2,2}\Phi_{3,1} + \Phi_{1,3}\Phi_{2,1}\Phi_{3,2} + \Phi_{1,2}\Phi_{2,3}\Phi_{3,1}) \right. \\
+ \Phi_{1,1}\Phi_{2,3}\Phi_{3,2} + \Phi_{1,2}\Phi_{2,1}\Phi_{3,3} + \Phi_{1,1}\Phi_{2,2}\Phi_{3,3}) \\
\left. + \hat{Y}_2(\tau) (\Phi_{1,1}\Phi_{2,1}\Phi_{3,1} + \Phi_{1,2}\Phi_{2,2}\Phi_{3,2} + \Phi_{1,3}\Phi_{2,3}\Phi_{3,3}) \right], \quad (63)
\end{aligned}$$

where λ is a constant to be fixed, χ_β are (gauge and flavour) singlets, $\Phi_{\alpha,p}$ are the p -th component of the α -th triplet with modular weight $-2/3$ and \hat{Y}_i are the modular forms defined in Equation (15). As mentioned before, the fields $\Phi_{\alpha,p}$ and χ_β acquire VEVs to cancel the FI-term. Thus, defining

$$\begin{aligned}
\tilde{\lambda}_1 := \lambda \langle \chi_1 \rangle \langle \chi_2 \rangle [\langle \Phi_{1,3} \rangle \langle \Phi_{2,2} \rangle \langle \Phi_{3,1} \rangle + \langle \Phi_{1,3} \rangle \langle \Phi_{2,1} \rangle \langle \Phi_{3,2} \rangle + \langle \Phi_{1,2} \rangle \langle \Phi_{2,3} \rangle \langle \Phi_{3,1} \rangle \\
+ \langle \Phi_{1,1} \rangle \langle \Phi_{2,3} \rangle \langle \Phi_{3,2} \rangle + \langle \Phi_{1,2} \rangle \langle \Phi_{2,1} \rangle \langle \Phi_{3,3} \rangle + \langle \Phi_{1,1} \rangle \langle \Phi_{2,2} \rangle \langle \Phi_{3,3} \rangle], \quad (64a)
\end{aligned}$$

$$\tilde{\lambda}_2 := \lambda \langle \chi_1 \rangle \langle \chi_2 \rangle [\langle \Phi_{1,1} \rangle \langle \Phi_{2,1} \rangle \langle \Phi_{3,1} \rangle + \langle \Phi_{1,2} \rangle \langle \Phi_{2,2} \rangle \langle \Phi_{3,2} \rangle + \langle \Phi_{1,3} \rangle \langle \Phi_{2,3} \rangle \langle \Phi_{3,3} \rangle], \quad (64b)$$

Equation (63) takes the simplified form (25), i.e.

$$W_{\text{Yuk}} = -\frac{1}{\sqrt{2}} \tilde{\lambda}_1 \hat{Y}_1(\tau) + \tilde{\lambda}_2 \hat{Y}_2(\tau) + \dots$$

At leading order, this approximation includes 11 out of a set of $\mathcal{O}(100)$ matter fields. All additional states appear at higher orders and are hence further suppressed. This implies that their contributions to W_{Yuk} can be ignored at first order.

References

- [1] D. Bailin and A. Love, “Orbifold compactifications of string theory,” *Phys. Rept.* **315** (1999) 285–408.
- [2] O. Lebedev, H. P. Nilles, S. Raby, S. Ramos-Sánchez, M. Ratz, P. K. S. Vaudrevange, and A. Wingerter, “A Mini-landscape of exact MSSM spectra in heterotic orbifolds,” *Phys. Lett. B* **645** (2007) 88–94, [arXiv:hep-th/0611095](#).
- [3] H. P. Nilles, S. Ramos-Sánchez, P. K. S. Vaudrevange, and A. Wingerter, “The Orbifolder: A Tool to study the Low Energy Effective Theory of Heterotic Orbifolds,” *Comput. Phys. Commun.* **183** (2012) 1363–1380, [arXiv:1110.5229 \[hep-th\]](#).
- [4] Y. Olgún-Trejo, R. Pérez-Martínez, and S. Ramos-Sánchez, “Charting the flavor landscape of MSSM-like Abelian heterotic orbifolds,” *Phys. Rev.* **D98** no. 10, (2018) 106020, [arXiv:1808.06622 \[hep-th\]](#).
- [5] A. Baur, H. P. Nilles, A. Trautner, and P. K. Vaudrevange, “A String Theory of Flavor and \mathcal{CP} ,” *Nucl. Phys. B* **947** (2019) 114737, [arXiv:1908.00805 \[hep-th\]](#).
- [6] S. Ramos-Sánchez and M. Ratz, *Heterotic Orbifold Models*. Springer, 2024. [arXiv:2401.03125 \[hep-th\]](#).
- [7] S. L. Parameswaran, S. Ramos-Sánchez, and I. Zavala, “On Moduli Stabilisation and de Sitter Vacua in MSSM Heterotic Orbifolds,” *JHEP* **1101** (2011) 071, [arXiv:1009.3931 \[hep-th\]](#).
- [8] M. P. García del Moral, S. Parameswaran, N. Quiroz, and I. Zavala, “Anti-D3 branes and moduli in non-linear supergravity,” *JHEP* **10** (2017) 185, [arXiv:1707.07059 \[hep-th\]](#).
- [9] M. van Beest, J. Calderón-Infante, D. Mirfendereski, and I. Valenzuela, “Lectures on the Swampland Program in String Compactifications,” *Phys. Rept.* **989** (2022) 1–50, [arXiv:2102.01111 \[hep-th\]](#).
- [10] M. Graña and A. Herráez, “The Swampland Conjectures: A Bridge from Quantum Gravity to Particle Physics,” *Universe* **7** no. 8, (2021) 273, [arXiv:2107.00087 \[hep-th\]](#).
- [11] Y. Olgún-Trejo, S. L. Parameswaran, G. Tasinato, and I. Zavala, “Runaway Quintessence, Out of the Swampland,” *JCAP* **01** (2019) 031, [arXiv:1810.08634 \[hep-th\]](#).
- [12] S. K. Garg and C. Krishnan, “Bounds on Slow Roll and the de Sitter Swampland,” *JHEP* **11** (2019) 075, [arXiv:1807.05193 \[hep-th\]](#).
- [13] H. Ooguri, E. Palti, G. Shiu, and C. Vafa, “Distance and de Sitter Conjectures on the Swampland,” *Phys. Lett. B* **788** (2019) 180–184, [arXiv:1810.05506 \[hep-th\]](#).

- [14] E. Gonzalo, L. E. Ibáñez, and Á. M. Uranga, “Modular symmetries and the swampland conjectures,” *JHEP* **05** (2019) 105, [arXiv:1812.06520 \[hep-th\]](#).
- [15] D. van de Heisteeg, C. Vafa, and M. Wiesner, “Bounds on Species Scale and the Distance Conjecture,” *Fortsch. Phys.* **71** no. 10-11, (2023) 2300143, [arXiv:2303.13580 \[hep-th\]](#).
- [16] A. Castellano, A. Herráez, and L. E. Ibáñez, “On the species scale, modular invariance and the gravitational EFT expansion,” *JHEP* **12** (2024) 019, [arXiv:2310.07708 \[hep-th\]](#).
- [17] D. van de Heisteeg, C. Vafa, M. Wiesner, and D. H. Wu, “Species scale in diverse dimensions,” *JHEP* **05** (2024) 112, [arXiv:2310.07213 \[hep-th\]](#).
- [18] R. Schimmrigk, “Automorphic inflation,” *Phys. Lett. B* **748** (2015) 376–379, [arXiv:1412.8537 \[hep-th\]](#).
- [19] R. Schimmrigk, “Modular Inflation Observables and j -Inflation Phenomenology,” *JHEP* **09** (2017) 043, [arXiv:1612.09559 \[hep-th\]](#).
- [20] R. Schimmrigk, “Large and small field inflation from hyperbolic sigma models,” *Phys. Rev. D* **105** no. 6, (2022) 063541, [arXiv:2108.05400 \[hep-th\]](#).
- [21] T. Kobayashi, D. Nitta, and Y. Urakawa, “Modular invariant inflation,” *JCAP* **08** (2016) 014, [arXiv:1604.02995 \[hep-th\]](#).
- [22] Y. Abe, T. Higaki, F. Kaneko, T. Kobayashi, and H. Otsuka, “Moduli inflation from modular flavor symmetries,” *JHEP* **06** (2023) 187, [arXiv:2303.02947 \[hep-ph\]](#).
- [23] S. F. King and X. Wang, “Modular invariant hilltop inflation,” *JCAP* **07** (2024) 073, [arXiv:2405.08924 \[hep-ph\]](#).
- [24] G.-J. Ding, S.-Y. Jiang, and W. Zhao, “Modular invariant slow roll inflation,” *JCAP* **10** (2024) 016, [arXiv:2405.06497 \[hep-ph\]](#).
- [25] G. F. Casas and L. E. Ibáñez, “Modular invariant Starobinsky inflation and the Species Scale,” *JHEP* **04** (2025) 041, [arXiv:2407.12081 \[hep-th\]](#).
- [26] S. Aoki and H. Otsuka, “Inflationary constraints on the moduli-dependent species scale in modular invariant theories,” [arXiv:2411.08467 \[hep-th\]](#).
- [27] R. Kallosh and A. Linde, “Landscape of modular cosmology,” *JCAP* **05** (2025) 037, [arXiv:2411.07552 \[hep-th\]](#).
- [28] R. Kallosh and A. Linde, “ $SL(2, \mathbb{Z})$ cosmological attractors,” *JCAP* **04** (2025) 045, [arXiv:2408.05203 \[hep-th\]](#).

- [29] **DESI** Collaboration, K. Lodha *et al.*, “DESI 2024: Constraints on physics-focused aspects of dark energy using DESI DR1 BAO data,” *Phys. Rev. D* **111** no. 2, (2025) 023532, [arXiv:2405.13588](#) [[astro-ph.CO](#)].
- [30] **DESI** Collaboration, A. G. Adame *et al.*, “DESI 2024 VI: cosmological constraints from the measurements of baryon acoustic oscillations,” *JCAP* **02** (2025) 021, [arXiv:2404.03002](#) [[astro-ph.CO](#)].
- [31] **DESI** Collaboration, M. Abdul Karim *et al.*, “DESI DR2 Results I: Baryon Acoustic Oscillations from the Lyman Alpha Forest,” [arXiv:2503.14739](#) [[astro-ph.CO](#)].
- [32] **DESI** Collaboration, M. Abdul Karim *et al.*, “DESI DR2 Results II: Measurements of Baryon Acoustic Oscillations and Cosmological Constraints,” [arXiv:2503.14738](#) [[astro-ph.CO](#)].
- [33] K. Lodha *et al.*, “Extended Dark Energy analysis using DESI DR2 BAO measurements,” [arXiv:2503.14743](#) [[astro-ph.CO](#)].
- [34] **DES** Collaboration, T. M. C. Abbott *et al.*, “The Dark Energy Survey: Cosmology Results with ~ 1500 New High-redshift Type Ia Supernovae Using the Full 5 yr Data Set,” *Astrophys. J. Lett.* **973** no. 1, (2024) L14, [arXiv:2401.02929](#) [[astro-ph.CO](#)].
- [35] **DES** Collaboration, T. M. C. Abbott *et al.*, “Dark Energy Survey: implications for cosmological expansion models from the final DES Baryon Acoustic Oscillation and Supernova data,” [arXiv:2503.06712](#) [[astro-ph.CO](#)].
- [36] B. Ratra and P. J. E. Peebles, “Cosmological Consequences of a Rolling Homogeneous Scalar Field,” *Phys. Rev. D* **37** (1988) 3406.
- [37] P. J. E. Peebles and B. Ratra, “Cosmology with a Time Variable Cosmological Constant,” *Astrophys. J. Lett.* **325** (1988) L17.
- [38] R. R. Caldwell, R. Dave, and P. J. Steinhardt, “Cosmological imprint of an energy component with general equation of state,” *Phys. Rev. Lett.* **80** (1998) 1582–1585, [arXiv:astro-ph/9708069](#).
- [39] D. Andriot, S. Parameswaran, D. Tsimpis, T. Wrase, and I. Zavala, “Exponential quintessence: curved, steep and stringy?,” *JHEP* **08** (2024) 117, [arXiv:2405.09323](#) [[hep-th](#)].
- [40] S. Bhattacharya, G. Borghetto, A. Malhotra, S. Parameswaran, G. Tasinato, and I. Zavala, “Cosmological constraints on curved quintessence,” *JCAP* **09** (2024) 073, [arXiv:2405.17396](#) [[astro-ph.CO](#)].

- [41] S. Bhattacharya, G. Borghetto, A. Malhotra, S. Parameswaran, G. Tasinato, and I. Zavala, “Cosmological tests of quintessence in quantum gravity,” *JCAP* **04** (2025) 086, [arXiv:2410.21243 \[astro-ph.CO\]](#).
- [42] H. Bernardo, R. Brandenberger, and J. Fröhlich, “Towards a dark sector model from string theory,” *JCAP* **09** (2022) 040, [arXiv:2201.04668 \[hep-th\]](#).
- [43] L. A. Anchordoqui, I. Antoniadis, N. Cribiori, A. Hasar, D. Lüst, J. Masias, and M. Scalisi, “Bulk/boundary Modular Quintessence and DESI,” [arXiv:2506.02731 \[hep-th\]](#).
- [44] A. Bedroya, G. Obied, C. Vafa, and D. H. Wu, “Evolving Dark Sector and the Dark Dimension Scenario,” [arXiv:2507.03090 \[astro-ph.CO\]](#).
- [45] F. Feruglio, “Are neutrino masses modular forms?,” in *From My Vast Repertoire ...: Guido Altarelli’s Legacy*, A. Levy, S. Forte, and G. Ridolfi, eds., pp. 227–266. 2019. [arXiv:1706.08749 \[hep-ph\]](#).
- [46] A. Baur, H. P. Nilles, S. Ramos-Sánchez, A. Trautner, and P. K. S. Vaudrevange, “The eclectic flavor symmetries of T^2/\mathbb{Z}_K orbifolds,” *JHEP* **09** (2024) 159, [arXiv:2405.20378 \[hep-th\]](#).
- [47] A. Baur, H. P. Nilles, A. Trautner, and P. K. Vaudrevange, “Unification of Flavor, CP, and Modular Symmetries,” *Phys. Lett. B* **795** (2019) 7–14, [arXiv:1901.03251 \[hep-th\]](#).
- [48] H. P. Nilles, S. Ramos-Sánchez, and P. K. Vaudrevange, “Eclectic Flavor Groups,” *JHEP* **02** (2020) 045, [arXiv:2001.01736 \[hep-ph\]](#).
- [49] H. P. Nilles, S. Ramos-Sánchez, and P. K. S. Vaudrevange, “Eclectic flavor scheme from ten-dimensional string theory - II. Detailed technical analysis,” *Nucl. Phys. B* **966** (2021) 115367, [arXiv:2010.13798 \[hep-th\]](#).
- [50] J. Lauer, J. Mas, and H. P. Nilles, “Duality and the Role of Nonperturbative Effects on the World Sheet,” *Phys. Lett.* **B226** (1989) 251–256.
- [51] J. Lauer, J. Mas, and H. P. Nilles, “Twisted sector representations of discrete background symmetries for two-dimensional orbifolds,” *Nucl. Phys.* **B351** (1991) 353–424.
- [52] H. P. Nilles, S. Ramos-Sánchez, and P. K. Vaudrevange, “Lessons from eclectic flavor symmetries,” *Nucl. Phys. B* **957** (2020) 115098, [arXiv:2004.05200 \[hep-ph\]](#).
- [53] A. Baur, H. P. Nilles, S. Ramos-Sánchez, A. Trautner, and P. K. S. Vaudrevange, “The first string-derived eclectic flavor model with realistic phenomenology,” *JHEP* **09** (2022) 224, [arXiv:2207.10677 \[hep-ph\]](#).

- [54] A. Baur, H. P. Nilles, S. Ramos-Sánchez, A. Trautner, and P. K. S. Vaudrevange, “Top-down anatomy of flavor symmetry breakdown,” *Phys. Rev. D* **105** no. 5, (2022) 055018, [arXiv:2112.06940 \[hep-th\]](#).
- [55] J. M. Leedom, N. Righi, and A. Westphal, “Heterotic de Sitter beyond modular symmetry,” *JHEP* **02** (2023) 209, [arXiv:2212.03876 \[hep-th\]](#).
- [56] S. Chen, D. van de Heisteeg, and C. Vafa, “Symmetries and M-theory-like Vacua in Four Dimensions,” [arXiv:2503.16599 \[hep-th\]](#).
- [57] D. Andriot, “Tachyonic de Sitter Solutions of 10d Type II Supergravities,” *Fortsch. Phys.* **69** no. 7, (2021) 2100063, [arXiv:2101.06251 \[hep-th\]](#).
- [58] D. Andriot and F. Ruehle, “On classical de Sitter solutions and parametric control,” *JHEP* **06** (2024) 101, [arXiv:2403.07065 \[hep-th\]](#).
- [59] S. Parameswaran and M. Serra, “On (A)dS solutions from Scherk-Schwarz orbifolds,” *JHEP* **10** (2024) 039, [arXiv:2407.16781 \[hep-th\]](#).
- [60] B. Valeixo Bento and M. Montero, “An M-theory dS maximum from Casimir energies on Riemann-flat manifolds,” [arXiv:2507.02037 \[hep-th\]](#).
- [61] M. Cicoli, G. Dibitetto, and F. G. Pedro, “Out of the Swampland with Multifield Quintessence?,” *JHEP* **10** (2020) 035, [arXiv:2007.11011 \[hep-th\]](#).
- [62] Y. Akrami, M. Sasaki, A. R. Solomon, and V. Vardanyan, “Multi-field dark energy: Cosmic acceleration on a steep potential,” *Phys. Lett. B* **819** (2021) 136427, [arXiv:2008.13660 \[astro-ph.CO\]](#).
- [63] L. Anguelova, J. Dumancic, R. Gass, and L. C. R. Wijewardhana, “Dark energy from inspiraling in field space,” *JCAP* **03** no. 03, (2022) 018, [arXiv:2111.12136 \[hep-th\]](#).
- [64] L. Anguelova, J. Dumancic, R. Gass, and L. C. R. Wijewardhana, “Dynamics of inspiraling dark energy,” *Eur. Phys. J. C* **84** no. 4, (2024) 365, [arXiv:2311.07839 \[hep-th\]](#).
- [65] J. R. Eskilt, Y. Akrami, A. R. Solomon, and V. Vardanyan, “Cosmological dynamics of multifield dark energy,” *Phys. Rev. D* **106** no. 2, (2022) 023512, [arXiv:2201.08841 \[astro-ph.CO\]](#).
- [66] M.-S. Seo, “Asymptotic Behavior of Saxon–Axion System in Stringy Quintessence Model,” *Fortsch. Phys.* **72** no. 11, (2024) 2400112, [arXiv:2403.07307 \[hep-th\]](#).
- [67] D. Licciardello, S. Rahimy, and I. Zavala, “Extending the Dynamical Systems Toolkit: Coupled Fields in Multiscalar Dark Energy,” [arXiv:2509.02539 \[hep-th\]](#).

- [68] W. Buchmüller, K. Hamaguchi, O. Lebedev, and M. Ratz, “Supersymmetric Standard Model from the Heterotic String (II),” *Nucl. Phys.* **B785** (2007) 149–209, [arXiv:hep-th/0606187](#) [hep-th].
- [69] H. P. Nilles and P. K. S. Vaudrevange, “Geography of Fields in Extra Dimensions: String Theory Lessons for Particle Physics,” *Mod. Phys. Lett.* **A30** no. 10, (2015) 1530008, [arXiv:1403.1597](#) [hep-th].
- [70] E. Parr and P. K. S. Vaudrevange, “Contrast data mining for the MSSM from strings,” *Nucl. Phys.* **B952** (2020) 114922, [arXiv:1910.13473](#) [hep-th].
- [71] F. Plöger, S. Ramos-Sánchez, M. Ratz, and P. K. S. Vaudrevange, “Mirage torsion,” *JHEP* **04** (2007) 063, [hep-th/0702176](#).
- [72] S. Ramos-Sánchez, “Towards Low Energy Physics from the Heterotic String,” *Fortsch. Phys.* **10** (2009) 907–1036, [arXiv:0812.3560](#) [hep-th].
- [73] P. K. S. Vaudrevange, “Grand Unification in the Heterotic Brane World,” [arXiv:0812.3503](#) [hep-th].
- [74] K.-S. Choi and J. E. Kim, “Quarks and Leptons From Orbifolded Superstring,” *Lect. Notes Phys.* **954** (2020) pp.
- [75] S. Ferrara, D. Lüst, A. D. Shapere, and S. Theisen, “Modular Invariance in Supersymmetric Field Theories,” *Phys. Lett.* **B225** (1989) 363.
- [76] A. Font, L. E. Ibáñez, D. Lüst, and F. Quevedo, “Supersymmetry breaking from duality invariant gaugino condensation,” *Phys. Lett.* **B245** (1990) 401–408.
- [77] M. Cvetič, A. Font, L. E. Ibáñez, D. Lüst, and F. Quevedo, “Target space duality, supersymmetry breaking and the stability of classical string vacua,” *Nucl. Phys. B* **361** (1991) 194–232.
- [78] P. Paradisi, M. Ratz, R. Schieren, and C. Simonetto, “Running minimal flavor violation,” *Phys. Lett.* **B668** (2008) 202–209, [arXiv:0805.3989](#) [hep-ph].
- [79] X.-G. Liu and G.-J. Ding, “Modular flavor symmetry and vector-valued modular forms,” *JHEP* **03** (2022) 123, [arXiv:2112.14761](#) [hep-ph].
- [80] G.-J. Ding, X.-G. Liu, J.-N. Lu, and M.-H. Weng, “Modular binary octahedral symmetry for flavor structure of Standard Model,” *JHEP* **11** (2023) 083, [arXiv:2307.14926](#) [hep-ph].
- [81] C. Arriaga-Osante, X.-G. Liu, and S. Ramos-Sánchez, “Quark and lepton modular models from the binary dihedral flavor symmetry,” *JHEP* **05** (2024) 119, [arXiv:2311.10136](#) [hep-ph].

- [82] C. Arriaga-Osante, M.-C. Chen, R. Díaz-Castro, X. Li, X.-G. Liu, S. Ramos-Sánchez, and M. Ratz, “Multiple realizations of modular flavor symmetries and their phenomenology,” *JHEP* **06** (2025) 096, [arXiv:2502.12270 \[hep-ph\]](#).
- [83] K. S. Narain, “New Heterotic String Theories in Uncompactified Dimensions < 10 ,” *Phys. Lett. B* **169** (1986) 41–46.
- [84] S. Groot Nibbelink and P. K. S. Vaudrevange, “T-duality orbifolds of heterotic Narain compactifications,” *JHEP* **04** (2017) 030, [arXiv:1703.05323 \[hep-th\]](#).
- [85] The GAP Group, *GAP – Groups, Algorithms, and Programming, Version 4.14.0*, 2024. <https://www.gap-system.org>.
- [86] L. E. Ibáñez and D. Lüst, “Duality anomaly cancellation, minimal string unification and the effective low-energy Lagrangian of 4-D strings,” *Nucl. Phys.* **B382** (1992) 305–361, [arXiv:hep-th/9202046 \[hep-th\]](#).
- [87] Y. Olguín-Trejo and S. Ramos-Sánchez, “Kähler potential of heterotic orbifolds with multiple Kähler moduli,” *J. Phys. Conf. Ser.* **912** no. 1, (2017) 012029, [arXiv:1707.09966 \[hep-th\]](#).
- [88] J.-N. Lu, X.-G. Liu, and G.-J. Ding, “Modular symmetry origin of texture zeros and quark lepton unification,” [arXiv:1912.07573 \[hep-ph\]](#).
- [89] J. Erler, D. Jungnickel, M. Spalinski, and S. Stieberger, “Higher twisted sector couplings of $z(n)$ orbifolds,” *Nucl. Phys.* **B397** (1993) 379–416, [hep-th/9207049](#).
- [90] S. Stieberger, “Moduli and twisted sector dependence on $Z(N) \times Z(M)$ orbifold couplings,” *Phys. Lett. B* **300** (1993) 347–353, [arXiv:hep-th/9211027](#).
- [91] M. Fischer, M. Ratz, J. Torrado, and P. K. S. Vaudrevange, “Classification of symmetric toroidal orbifolds,” *JHEP* **01** (2013) 084, [arXiv:1209.3906 \[hep-th\]](#).
- [92] T. Kobayashi, S. Raby, and R.-J. Zhang, “Constructing 5d orbifold grand unified theories from heterotic strings,” *Phys. Lett.* **B593** (2004) 262–270, [hep-ph/0403065](#).
- [93] T. Kobayashi, S. Raby, and R.-J. Zhang, “Searching for realistic 4d string models with a Pati-Salam symmetry: Orbifold grand unified theories from heterotic string compactification on a $Z(6)$ orbifold,” *Nucl. Phys. B* **704** (2005) 3–55, [arXiv:hep-ph/0409098](#).
- [94] O. Lebedev, H. P. Nilles, S. Ramos-Sánchez, M. Ratz, and P. K. S. Vaudrevange, “Heterotic mini-landscape (II): completing the search for MSSM vacua in a Z_6 orbifold,” *Phys. Lett.* **B668** (2008) 331–335, [arXiv:0807.4384 \[hep-th\]](#).

- [95] D. Bailin, A. Love, W. A. Sabra, and S. Thomas, “Modular symmetries in $Z(N)$ orbifold compactified string theories with Wilson lines,” *Mod. Phys. Lett. A* **9** (1994) 1229–1238, [arXiv:hep-th/9312122](#).
- [96] A. Love and S. Todd, “Modular symmetries of threshold corrections for Abelian orbifolds with discrete Wilson lines,” *Nucl. Phys. B* **481** (1996) 253–288, [arXiv:hep-th/9606161](#).
- [97] P. Fayet and J. Iliopoulos, “Spontaneously Broken Supergauge Symmetries and Goldstone Spinors,” *Phys. Lett. B* **51** (1974) 461–464.
- [98] O. Lebedev, H. P. Nilles, S. Raby, S. Ramos-Sánchez, M. Ratz, P. K. S. Vaudrevange, and A. Wingerter, “The Heterotic Road to the MSSM with R parity,” *Phys. Rev. D* **77** (2008) 046013, [arXiv:0708.2691 \[hep-th\]](#).
- [99] F. Brümmer, R. Kappl, M. Ratz, and K. Schmidt-Hoberg, “Approximate R-symmetries and the mu term,” *JHEP* **04** (2010) 006, [arXiv:1003.0084 \[hep-ph\]](#).
- [100] R. Kappl, B. Petersen, S. Raby, M. Ratz, R. Schieren, and P. K. Vaudrevange, “String-derived MSSM vacua with residual R symmetries,” *Nucl.Phys.* **B847** (2011) 325–349, [arXiv:1012.4574 \[hep-th\]](#).
- [101] V. Knapp-Pérez, X.-G. Liu, H. P. Nilles, S. Ramos-Sánchez, and M. Ratz, “Matter matters in moduli fixing and modular flavor symmetries,” *Phys. Lett. B* **844** (2023) 138106, [arXiv:2304.14437 \[hep-th\]](#).
- [102] J. P. Derendinger, S. Ferrara, C. Kounnas, and F. Zwirner, “On loop corrections to string effective field theories: Field dependent gauge couplings and sigma model anomalies,” *Nucl. Phys.* **B372** (1992) 145–188.
- [103] A. Font, L. E. Ibáñez, H. P. Nilles, and F. Quevedo, “Degenerate Orbifolds,” *Nucl. Phys. B* **307** (1988) 109–129. [Erratum: *Nucl.Phys.B* 310, 764–764 (1988)].
- [104] A. Font, L. E. Ibáñez, H. P. Nilles, and F. Quevedo, “On the Concept of Naturalness in String Theories,” *Phys. Lett. B* **213** (1988) 274–278.
- [105] T. Kobayashi, S. L. Parameswaran, S. Ramos-Sánchez, and I. Zavala, “Revisiting Coupling Selection Rules in Heterotic Orbifold Models,” *JHEP* **05** (2012) 008, [arXiv:1107.2137 \[hep-th\]](#). [Erratum: *JHEP*12,049(2012)].
- [106] T. Kobayashi, R. Nishida, and H. Otsuka, “Non-Invertible Selection Rules on Heterotic Non-Abelian Orbifolds,” [arXiv:2509.10019 \[hep-th\]](#).
- [107] E. J. Chun, J. Mas, J. Lauer, and H. P. Nilles, “Duality and Landau-Ginzburg Models,” *Phys. Lett.* **B233** (1989) 141–146.

- [108] H. Rademacher and H. S. Zuckerman, “On the fourier coefficients of certain modular forms of positive dimension,” *Annals of Mathematics* **39** no. 2, (1938) 433–462.
- [109] J. Lehner, *Discontinuous Groups and Automorphic Functions*. Mathematical surveys and monographs. American Mathematical Society, 1964.
- [110] S. H. Shenker, “The Strength of nonperturbative effects in string theory,”. Presented at the Cargese Workshop on Random Surfaces, Quantum Gravity and Strings, Cargese, France, May 28 - Jun 1, 1990.
- [111] F. F. Gautason, M. Schillo, T. Van Riet, and M. Williams, “Remarks on scale separation in flux vacua,” *JHEP* **03** (2016) 061, [arXiv:1512.00457 \[hep-th\]](#).
- [112] D. Lüst, E. Palti, and C. Vafa, “AdS and the Swampland,” *Phys. Lett. B* **797** (2019) 134867, [arXiv:1906.05225 \[hep-th\]](#).
- [113] M. Demirtas, M. Kim, L. McAllister, J. Moritz, and A. Rios-Tascon, “Small cosmological constants in string theory,” *JHEP* **12** (2021) 136, [arXiv:2107.09064 \[hep-th\]](#).
- [114] M. Demirtas, M. Kim, L. McAllister, J. Moritz, and A. Rios-Tascon, “Exponentially Small Cosmological Constant in String Theory,” *Phys. Rev. Lett.* **128** no. 1, (2022) 011602, [arXiv:2107.09065 \[hep-th\]](#).
- [115] T. Coudarchet, “Hiding the extra dimensions: A review on scale separation in string theory,” *Phys. Rept.* **1064** (2024) 1–28, [arXiv:2311.12105 \[hep-th\]](#).
- [116] D. Andriot, N. Cribiori, and T. Van Riet, “Scale separation, rolling solutions and entropy bounds,” [arXiv:2504.08634 \[hep-th\]](#).
- [117] G. Tringas and T. Wrase, “Scale separation from O-planes,” [arXiv:2504.15436 \[hep-th\]](#).
- [118] A. Proust, H. Samtleben, and E. Sezgin, “Scale separation on $\text{AdS}_3 \times S^3$ with and without supersymmetry,” [arXiv:2504.12425 \[hep-th\]](#).
- [119] G. Shiu, F. Tonioni, V. Van Hemelryck, and T. Van Riet, “AdS scale separation and the distance conjecture,” *JHEP* **05** (2023) 077, [arXiv:2212.06169 \[hep-th\]](#).
- [120] P. Svrček and E. Witten, “Axions in string theory,” *JHEP* **06** (2006) 051, [hep-th/0605206](#).
- [121] S. Dutta and R. J. Scherrer, “Hilltop Quintessence,” *Phys. Rev. D* **78** (2008) 123525, [arXiv:0809.4441 \[astro-ph\]](#).
- [122] **Planck** Collaboration, N. Aghanim *et al.*, “Planck 2018 results. VI. Cosmological parameters,” *Astron. Astrophys.* **641** (2020) A6, [arXiv:1807.06209 \[astro-ph.CO\]](#). [Erratum: *Astron. Astrophys.* 652, C4 (2021)].

- [123] P. P. Novichkov, J. T. Penedo, and S. T. Petcov, “Fermion Mass Hierarchies, Large Lepton Mixing and Residual Modular Symmetries,” [arXiv:2102.07488](#) [[hep-ph](#)].
- [124] F. Feruglio, V. Gherardi, A. Romanino, and A. Titov, “Modular invariant dynamics and fermion mass hierarchies around $\tau = i$,” *JHEP* **05** (2021) 242, [arXiv:2101.08718](#) [[hep-ph](#)].
- [125] H. Ooguri and C. Vafa, “On the Geometry of the String Landscape and the Swampland,” *Nucl. Phys. B* **766** (2007) 21–33, [arXiv:hep-th/0605264](#).
- [126] M. Chevallier and D. Polarski, “Accelerating universes with scaling dark matter,” *Int. J. Mod. Phys. D* **10** (2001) 213–224, [arXiv:gr-qc/0009008](#).
- [127] E. V. Linder, “Exploring the expansion history of the universe,” *Phys. Rev. Lett.* **90** (2003) 091301, [arXiv:astro-ph/0208512](#).
- [128] T. Chiba, “Slow-Roll Thawing Quintessence,” *Phys. Rev. D* **79** (2009) 083517, [arXiv:0902.4037](#) [[astro-ph.CO](#)]. [Erratum: *Phys.Rev.D* 80, 109902 (2009)].
- [129] A. A. Sen, S. A. Adil, and S. Sen, “Do cosmological observations allow a negative Λ ?,” *Mon. Not. Roy. Astron. Soc.* **518** no. 1, (2022) 1098–1105, [arXiv:2112.10641](#) [[astro-ph.CO](#)].
- [130] S. A. Adil, U. Mukhopadhyay, A. A. Sen, and S. Vagnozzi, “Dark energy in light of the early JWST observations: case for a negative cosmological constant?,” *JCAP* **10** (2023) 072, [arXiv:2307.12763](#) [[astro-ph.CO](#)].
- [131] N. Menci, S. A. Adil, U. Mukhopadhyay, A. A. Sen, and S. Vagnozzi, “Negative cosmological constant in the dark energy sector: tests from JWST photometric and spectroscopic observations of high-redshift galaxies,” *JCAP* **07** (2024) 072, [arXiv:2401.12659](#) [[astro-ph.CO](#)].
- [132] H. Wang, Z.-Y. Peng, and Y.-S. Piao, “Can recent DESI BAO measurements accommodate a negative cosmological constant?,” *Phys. Rev. D* **111** no. 6, (2025) L061306, [arXiv:2406.03395](#) [[astro-ph.CO](#)].
- [133] **DESI** Collaboration, K. Lodha *et al.*, “Extended Dark Energy analysis using DESI DR2 BAO measurements,” [arXiv:2503.14743](#) [[astro-ph.CO](#)].
- [134] S. Das, P. S. Corasaniti, and J. Khoury, “Super-acceleration as signature of dark sector interaction,” *Phys. Rev. D* **73** (2006) 083509, [arXiv:astro-ph/0510628](#).